AD-A038 393 ARMY MOBILITY EQUIPMENT RESEARCH AND DEVELOPMENT COMM--ETC F/G 20/3
MEASUREMENTS OF AC LOSSES IN SUPERCONDUCTORS BELOW HC1.(U)
SEP 76 J T BROACH

UNCLASSIFIED MERADCOM-2191 NL

| OF |
AD
A038393

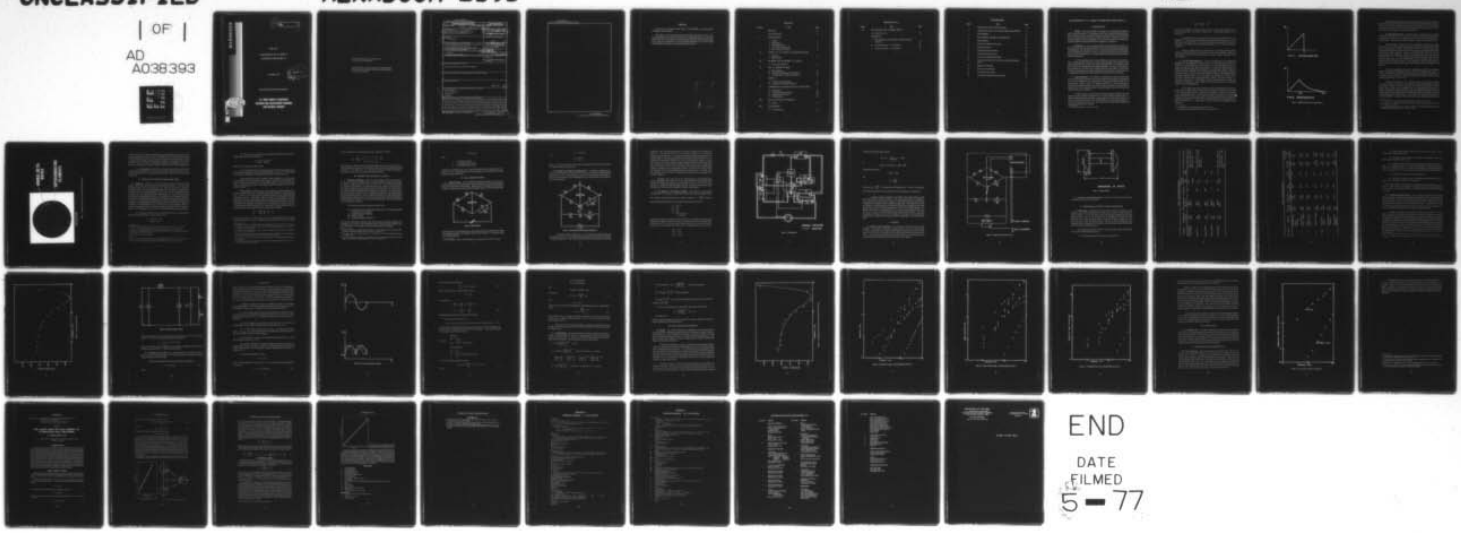

END

DATE
FILMED
5-77

(12) AD

Report 2191

MEASUREMENTS OF AC LOSSES IN SUPERCONDUCTORS BELOW H_{c1}

September 1976

U.S. ARMY MOBILITY EQUIPMENT
RESEARCH AND DEVELOPMENT COMMAND
FORT BELVOIR, VIRGINIA

Destroy this report when it is no longer needed.
Do not return it to the originator.

The citation in this report of trade names of commercially available products does not constitute official endorsement or approval of the use of such products.

UNCLASSIFIED

SECURITY CLASSIFICATION OF THIS PAGE *(When Data Entered)*

REPORT DOCUMENTATION PAGE	READ INSTRUCTIONS BEFORE COMPLETING FORM
1. REPORT NUMBER: 2191 — 2. GOVT ACCESSION NO.: 14 MERADCOM-2191	3. RECIPIENT'S CATALOG NUMBER
4. TITLE *(and Subtitle)*: MEASUREMENTS OF AC LOSSES IN SUPERCONDUCTORS BELOW H_{c1}	5. TYPE OF REPORT & PERIOD COVERED: Final; Jan 1974 ~~through~~ Jun 1976
	6. PERFORMING ORG. REPORT NUMBER
7. AUTHOR(s): J. Thomas Broach	8. CONTRACT OR GRANT NUMBER(s)
9. PERFORMING ORGANIZATION NAME AND ADDRESS: U.S. Army Mobility Equipment Research and Development Command, Electrical Power Laboratory, ATTN: DRDME-EA, Fort Belvoir, Virginia 22060	10. PROGRAM ELEMENT, PROJECT, TASK AREA & WORK UNIT NUMBERS: 62708A — 1G762708AH67 EA 045 CO6E197 EF CSS
11. CONTROLLING OFFICE NAME AND ADDRESS: U.S. Army Mobility Equipment Research and Development Command, Fort Belvoir, Virginia 22060	12. REPORT DATE: September 1976
	13. NUMBER OF PAGES: 48 — 46 pp
14. MONITORING AGENCY NAME & ADDRESS *(if different from Controlling Office)*	15. SECURITY CLASS. *(of this report)*: Unclassified
	15a. DECLASSIFICATION/DOWNGRADING SCHEDULE

16. DISTRIBUTION STATEMENT *(of this Report)*

Approved for public release; distribution unlimited.

17. DISTRIBUTION STATEMENT *(of the abstract entered in Block 20, if different from Report)*

18. SUPPLEMENTARY NOTES

403 160

19. KEY WORDS *(Continue on reverse side if necessary and identify by block number)*

Superconductors
AC Loss Mechanisms
Eddy Current
AC Bridge

20. ABSTRACT *(Continue on reverse side if necessary and identify by block number)*

An AC bridge technique is described for measuring energy losses in multifilament (MF) superconductors due to alternating current flow in superconducting solenoids. Superconductivity and transient loss theory are briefly discussed, and the apparatus used to measure the losses is described in detail. Loss data as a function of frequency in the field region $H < H_{c1}$ was obtained from measurements on a number of solenoids which were wound from commercially available MF NbTi conductors. Some data is presented in which an external field of $H > H_{c1}$ is applied.

DD FORM 1 JAN 73 1473 EDITION OF 1 NOV 65 IS OBSOLETE

UNCLASSIFIED

SECURITY CLASSIFICATION OF THIS PAGE *(When Data Entered)*

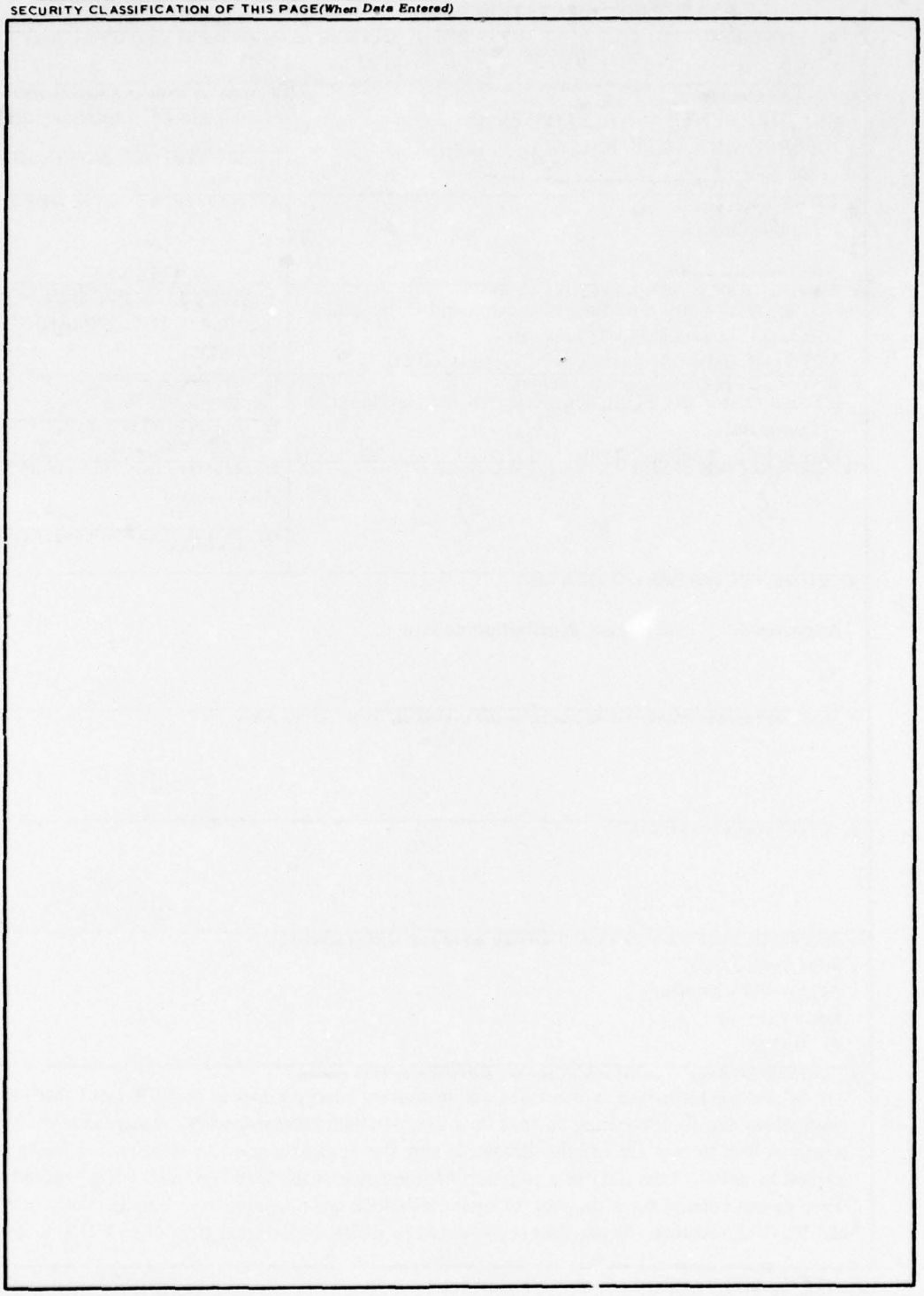

PREFACE

This work was authorized under Project 1G762708AH67, "Combat Support Technology Energy Systems."

The project was conceived in discussions the author had with Mr. James H. Ferrick and with Dr. Larry I. Amstutz who was also of considerable assistance in the initial phases of the effort. Mr. Harry W. Eisenhart, Engineering Technician, was instrumental in the design and construction of the experimental apparatus and in various repairs and modifications required as the experimental system evolved.

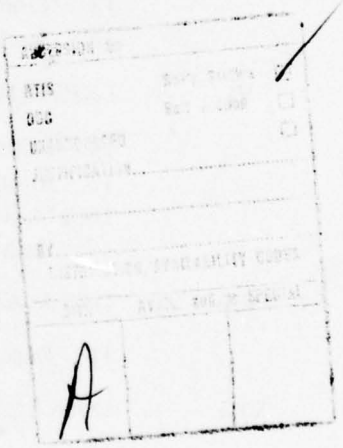

CONTENTS

CONTENTS (cont'd)

ILLUSTRATIONS

MEASUREMENTS OF AC LOSSES IN SUPERCONDUCTORS BELOW H_{c1}

I. INTRODUCTION

1. **General.** This report describes a technique for measuring energy losses in type II superconductors due to alternating current flow in superconducting solenoids. Superconductivity and the transient loss theory are briefly discussed, and the apparatus used to measure the losses is described in detail. Loss data as a function of frequency, which was obtained from measurements on a number of solenoids wound from commercially available multifilament (MF) NbTi conductors, is presented.

2. **Background.** A class of metallic conductor exists which when cooled to very low temperatures loses all electrical resistance. Such metals are called superconductors. This phenomena was first discovered in 1911 and was accompanied by glowing predictions of widespread application; however, it was soon discovered that this resistanceless property was destroyed by very small magnetic fields, eliminating typical electromagnetic applications.

In 1960, high-field, type II superconductors were discovered by Kunzler.[1] These superconductors remained in the superconducting state when exposed to high magnetic fields and high currents, and again superconductivity was considered as having a bright future of industrial and military applications. It is these type II superconductors which are the subject of the research described in this report. In spite of the favorable electromagnetic properties exhibited by these materials, no widespread, practical applications for them have been found in the 16 years since their discovery.

3. **Superconductivity.** The resistance of materials in the superconducting state is zero for all practical purposes. Recent measurements have placed an upper limit of 10^{-21} Ω on the resistivity of a superconductor. This compares with a value of 10^{-9} Ω for high-purity copper at 4.2K. The critical temperature, T_c, is the temperature at which a given material undergoes the transition from the normal to the superconducting state, but it is the magnetic behavior of superconductors which divides them into classes known as type I or type II.

A bulk specimen of metal in the superconducting state exhibits perfect diamagnetism with the magnetic induction $B = 0$. This is called the Meisner effect. In reality, a magnetic field can penetrate a small distance into a bulk superconductor. In the pure superconducting state, the only field allowed is exponentially damped as it goes in from an external surface with the strength of the field decreasing inward from the surface according to the relation

[1] J. E. Kunzler, *Rev. of Mod. Phy.*, Vol. 33, No. 1, 1961.

$$B(X) = B(O)\, e^{-\frac{X}{\lambda}}$$

where X is the distance in from the surface and λ is a characteristic length known as the penetration depth. This distance is quite small – a typical value being 5.0×10^{-6} cm for tin.[2]

A sufficiently strong magnetic field will destroy superconductivity. This threshold on critical value of the applied magnetic field is denoted by H_c and is referred to as the critical field. This value is dependent on temperature, but the value commonly used is either T = 0 for pure superconductors or T = 4.2 for practical superconductors.

There is an upper limit to the current which can be passed through a superconductor without driving the material back into its normal condition. There is a close relation between this critical current, I_c, and the magnetic properties of the superconductor.

4. Type II Superconductivity. There is no difference in the fundamental mechanism of superconductivity in type I and type II superconductors; however, the Meisner effect is quite different in the two types.[3] A type I superconductor (Figure 1) excludes a magnetic field until superconductivity is destroyed suddenly and completely, and then the field penetrates completely. A type II superconductor (Figure 1) excludes the field completely only in relatively weak fields up to a field H_{c1} called the lower critical field. Above H_{c1} the field is partially excluded, but the material remains electrically superconducting. At a much higher field, typically 6T to 120T, the flux penetrates completely and all superconductivity vanishes. This field is called H_{c2} – the upper, critical field. It is this ability of type II superconductors to remain electrically superconducting at high magnetic fields that makes them of considerable interest for practical applications.

In the region between H_{c1} and H_{c2}, a type II superconductor is said to be in the vortex, or mixed, state. In this state, flux penetrates the specimen as an array of flux tubes parallel to the field. Each flux tube consists of a normal core surrounded by a screening-current vortex. As the field is increased, the number of flux tubes increases until at the upper, critical field the normal regions overlap, and superconductivity is destroyed. The flux motion leads to hysteresis in the magnetization of type II materials and is a major source of power losses under alternating current conditions.

---

[2] G. G. Haseldenj, ed., *Cryogenic Fundamentals,* Academic Press, 1971.

[3] C. Kittel, *Introduction to Solid State Physics,* 4th ed., John Wiley & Sons, 1971.

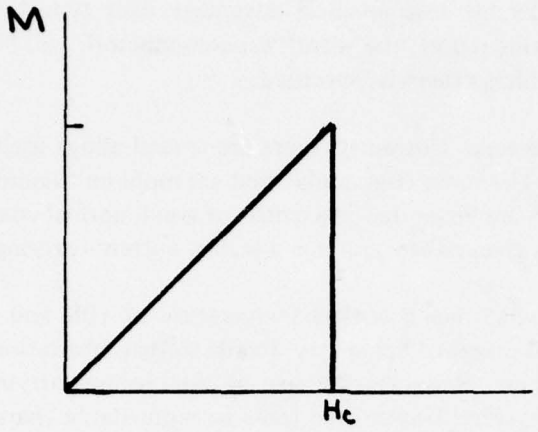

TYPE I SUPERCONDUCTOR

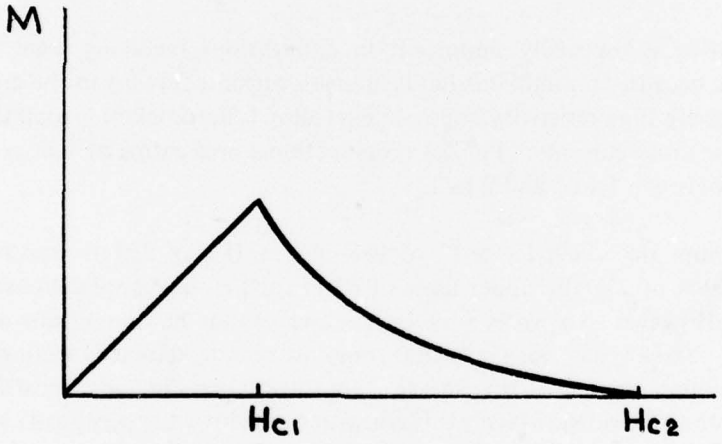

TYPE II SUPERCONDUCTOR

Figure 1. Magnetization curves of superconductors.

Most useful superconductors for technological purposes are type II materials. Superconductors in this class have the highest values of critical temperature, field, and current and thus offer considerable technological advantage over type I materials. Throughout the remainder of this report, the word "superconductor" will be used to mean type II superconductor unless otherwise specified.

5. **Practical Superconductors.** Currently, there are several alloys used to make commercial superconductors. The most commonly used are niobium titanium (NbTi) and niobium tin (Nb_3Sn) which are integrated in a matrix of good, normal conductor – usually copper. This matrix is essential to produce a stable, current-carrying wire.[4] [5]

Niobium titanium, which has a critical temperature of 10K and an upper critical field of 12T, has the advantage of being very ductile so that fabrication is easier and the superconductor cheaper. Reducing the size of the current-carrying, superconducting filaments reduces hysteresis losses and leads to more stable characteristics under transient field conditions. Because of its high ductility, NbTi can be easily manufactured in MF conductors. These are wires with many small superconducting filaments (Figure 2). The NbTi filaments have diameters typically in the range of 1-30 micrometers (μm), and over 1000 filaments can be incorporated in one wire approximately 0.015 inch in diameter. These filaments are usually twisted inside the matrix so that they spiral along the length of the conductor with a twist pitch of 1-10 per inch.

Twisting is especially important in applications involving large, transient magnetic fields because it eliminates induced cross currents flowing in the matrix.[6] A matrix of relatively high resistivity copper-nickel alloy (cupronickel) is sometimes used to impede these cross currents. Typical cross-sectional area ratios of matrix to superconductor are between 1 to 1 and 2 to 1.

Niobium tin which has a T_c of 18K and an H_{c2} of 25T is used in applications where fields of 7T (the upper limit of NbTi for practical applications) or more are required. However, Nb_3Sn is very brittle and cannot be drawn into wire form. Until recently, Nb_3Sn has been available only in rectangular-cross-section tape, or ribbon. This ribbon consists of Nb_3Sn a few μm thick laid on metallic substrate with a normal stabilizer as the outside layer; this construction allows the composite to be bent without damaging the superconductor. Coils made from Nb_3Sn tape are usually of the pancake variety. A pancake is simply a length of tape wound on a spool just as a

---

4 Z. J. J. Stekly, "State of the Art of Superconducting Magnets," *J. Appl. Phys.*, 42, p. 65, 1971.

5 M. N. Wilson, *et al.*, "Experimental and Theoretical Studies of Filamentary Superconducting Composites," *J. Phys., D*, Vol. 3, No. 11, 1970.

6 R. R. Critchlow, B. Zeitlin, and E. Gregory, "The Effect of Twist on AC Loss and Stability in Multistrand Superconducting Composites," *Appl. Phys. Lett.* Vol. 15, No. 7, 1969.

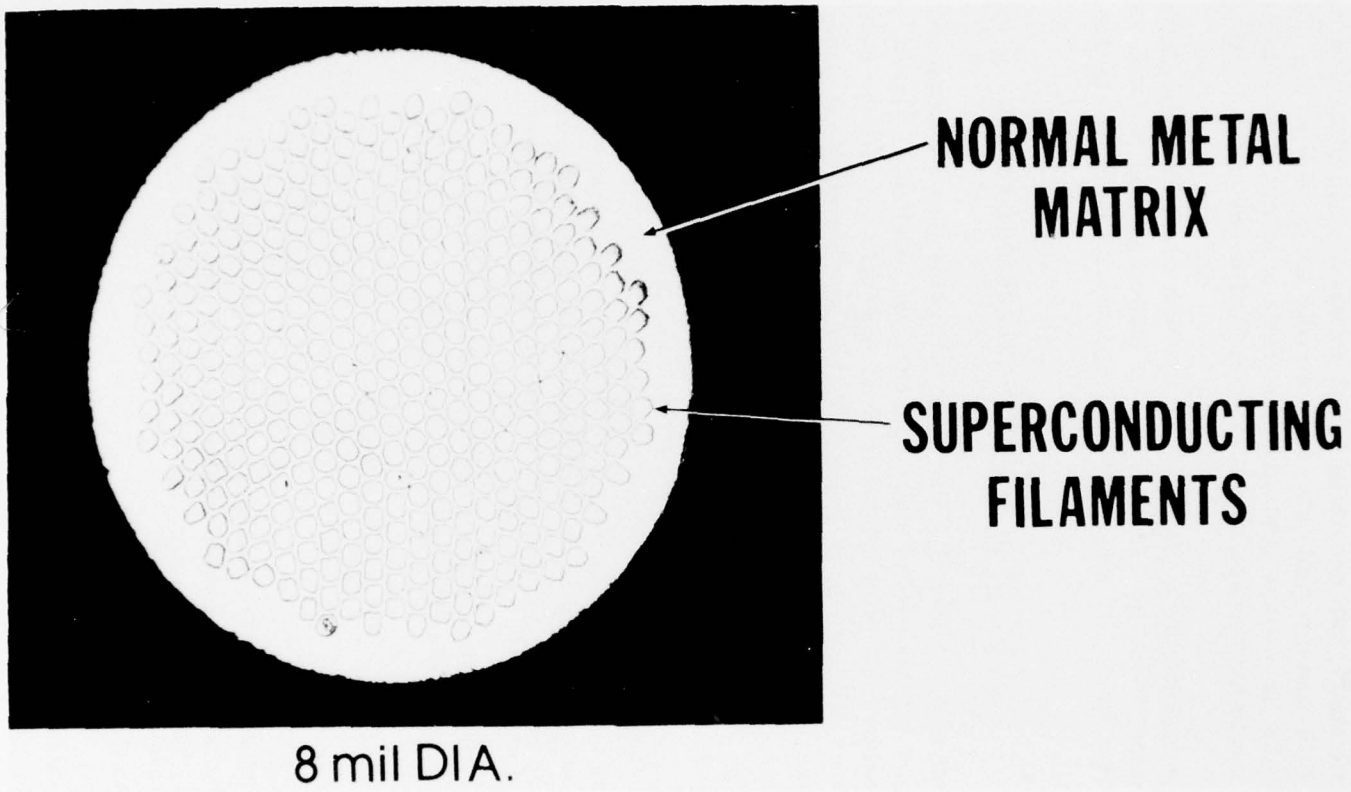

Figure 2. Enlarged cross section of commercial superconducting wire.

roll of scotch tape. To make a solenoid, many of these pancakes are stacked on top of one another and connected in series. Solenoids made from Nb_3Sn tapes have good high-field performance; but, not having the advantages of small filamentary twisted conductors, their transient field behavior is generally not as good as that of NbTi. Recently, Nb_3Sn has become commercially available in multifilament form, but at present this conductor is expensive and has been used in few practical applications.

A vanadium-gallium alloy, V_3Ga, is the most recent entry into the field of commercial superconductors. V_3Ga has even better high-field performance than Nb_3Sn; however, since it is relatively new and expensive, it has not been used in many applications.

II. THEORY OF AC LOSSES IN SUPERCONDUCTORS

6. Hysteresis. Above H_{c1}, the flux penetration into the superconducting material causes hysteresis losses under transient field conditions. The AC creates alternating fields in the superconductor so at high peak currents the material is constantly being driven around its magnetization cycle. Methods of calculating these hysteresis losses have been published,[7-10] and many of these methods are widely accepted today. The critical-state model due to Bean[11 12] is one of the more widely used methods for calculating these losses. The major flaw in the Bean and London[13] critical-state models is that they assume that the critical-current density of the superconductor, J_c, is independent of magnetic field and that the full-current density flows in regions of the superconductor where magnetic fields have penetrated. Clearly, the assumption of the independence of J_c on the field is not a valid assumption. However, using the assumptions of the critical-state model, the hysteresis losses in superconductors can be calcualted by any one of several fundamentally equivalent techniques:

(1) The power dissipated can be calculated from the area enclosed within the magnetic hysteresis loop, i.e., power loss per cycle is

$$P \propto \int_{\text{volume}} dV \int_{\text{cycle}} H \cdot dB.$$

---

[7] R. Hancox, "Calculation of AC Losses in a Type II Superconductor," *Proc IEEE*, Vol. 113, No. 7, 1966.

[8] H. London, "AC Losses in Superconductors of the Second Kind," *Phys Lett*, Vol. 6, No. 2, 1963.

[9] G. H. Morgan, "Theoretical Behavior of Multicore Superconducting Wire in a Time-Varying Uniform Magnetic Field," *J. Appl. Phys.*, Vol. 41, No. 9, 1970.

[10] C. P. Bean, *Phys. Rev, Lett.*, 8: 250 (1962).

[11] *Ibid.*

[12] G. Bogner and W. Heinzel, "Alternating Current Losses in Hard Superconductors," *S. St. Elec.*, Vol. 7, pp. 93-99.

[13] H. London, "AC Losses in Superconductors of the Second Kind," *Phys. Lett.*, Vol. 6, No. 2, 1963.

(2) The loss can be calculated by integrating the Poynting Vector over the sample surface and over a complete cycle,

$$P \propto \int_{\text{cycle}} dt \int_{\text{surface}} E \times H \, dA,$$

where dA is area element normal to surface.

(3) The electric field E is calculated as a function of position and time, and the local power dissipation is calculated by integrating $E \cdot J$ over a cycle. This method is quite useful in applications of the Bean Model in which J is either zero or J_c.

Other critical-state models including a field dependence of J_c have been developed; however, these models are more complex and will not be described in this report. Hysteresis losses have been experimentally shown to vary linearly with frequency and have revealed power losses proportional to the square or cube of the current and field.[14-18]

7. **Eddy Currents.** Another source of power losses in superconducting coils is the flow of eddy currents in the normally conducting stabilizer of superconducting wires. Copper is the most common stabilizer material; and at superconducting temperatures it has a conductivity 100 times greater than conductivity at room temperature; this high conductivity creates very favorable conditions for the flow of eddy currents when transient magnetic fields are experienced. These losses are readily calculated by the application of Faraday's law to the geometry of interest. If the case of a multifilament superconducting wire in a sinusoidal AC field is considered, one can obtain[19] an expression for the power loss per unit volume of stabilizer

$$\frac{\dot{Q}}{V} = \frac{2\pi \dot{B}^2}{V \rho} \int_0^x \frac{r_m^4}{4} \, dx'$$

where $\dot{Q}$ is the power, V is the volume, r_m is the maximum radius of eddy current loop (half the distance between S.C. filament), and ρ is the matrix resistivity. Carrying

---

[14] G. Bogner and W. Heinzel, "Alternating Current Losses in Hard Superconductors," *S. St. Elec.*, Vol. 7, pp. 93-99.

[15] G. H. Morgan, *et al.*, "Measurements of Energy Losses in Pulsed Superconducting Magnets," *J. Appl. Phys.*, Vol. 40, No. 4, pp. 1821-1829, 1964.

[16] W. T. Beall, Jr. and W. Meyerhoff, "AC Energy Losses Above and Below H_{c1} in Ni and NiZr," *J. Appl. Phys.*, Vol. 40, No. 5, pp. 2052-2059, 1969.

[17] D. Ho, M. C. Robinson, V. Srivastava, and R. Stevenson, "AC Loss as a Function of Current and External Magnetic Field in Commercial NbTi Superconductors," *Tech Rpt. AFML-TR-75-23.*

[18] W. J. Garr, Jr., M. S. Walker, D. W. Deis, and J. H. Murphy, "Hysteresis Loss in a Multifilament Superconductor," to be published.

[19] J. T. Broach and W. D. Lee, "The Application of Loss Models to Superconducting Solenoids," *Adv. in Cry. Eng.*, Vol. 19 (1974). (Included as Appendix A.)

out the calculation for an hcp filament structure (Appendix A), one has

$$\frac{\dot{Q}}{V} = \frac{\dot{B}^2 d^2}{8\rho} \frac{\frac{n^5}{5} + n^4 + n^3 + \frac{n}{8} + \frac{1}{160}}{\frac{n^3}{3} + n^2 + \frac{n}{2} + \frac{1}{24}} .$$

Both theoretical calculation and experimental data indicate that eddy current losses are proportional to the square of the frequency and the square of the transport current and field. In the region $H > H_{c1}$, eddy-current losses are usually dominated by hysteresis losses except in very high fields or high frequencies.

III. METHODS FOR MEASURING AC LOSSES

8. **Discussion of Methods.** There are several methods which have been used in recent years to measure transient losses in superconductors, and these can generally be classed as either thermal or electrical in nature.[20] [21] The most popular method is a thermal method known as the calorimetric (boil-off) method. In this technique, the sample is immersed in liquid helium, and the heat produced by the losses results in the boil off of liquid helium which is measured by a flowmeter. The measured flow rate is then related, through the heat of vaporization of helium, to the power losses in the superconducting sample. The low sensitivity (generally, a few mW) of this method usually dictates a sample of wire at least a few meters in length. The boil-off technique is especially suited for high loss rates and large samples since the lack of sensitivity causes no problems in this case.

There are several electrical methods commonly used:

(1) measurement of the current and voltage across the specimen along with the proper phase relationship
(2) mutual-inductance techniques
(3) bridge techniques
(4) electronic wattmeter methods.[22]

The electrical methods are generally more sensitive than the thermal methods; some investigators have claimed 1 μW sensitivities which are required when small loss rates are to be measured. For example, the wattmeter method gives a reading of

---

[20] D. Ho, M. C. Robinson, V. Srivastava, and R. Stevenson, "AC Loss as a Function of Current and External Magnetic Field in Commercial NbTi Superconductors," *Tech Rpt. AFML-TR-75-23.*

[21] S. L. Wipf, "AC Losses in Superconductors," *Proc. 1968 Summer Study on Superconducting Devices and Accelerators, Part II.*

[22] D. Ho, M. C. Robinson, V. Srivastava, and R. Stevenson, "AC Loss as a Function of Current and External Magnetic Field in Commercial NbTi Superconductors," *Tech Rpt. AFML-TR-75-23.*

$$P = IV \cos \phi$$

where

I = sample rms current
V = rms voltage across sample
ϕ = the angle between V and I.

In general, it is probably best to use a thermal method if loss rates are expected to be at least 1 watt or several watts while electrical methods are most suitable in measuring losses in the range of milliwatts.

IV. THE AC BRIDGE METHOD

9. Maxwell Bridge. An AC null-detecting bridge technique was used in the work described herein. This method was chosen mainly because of the high sensitivity provided in this null-detecting method. Many types of AC bridges were considered, but the one finally chosen was the Maxwell bridge[23] (Figure 3) which combines high

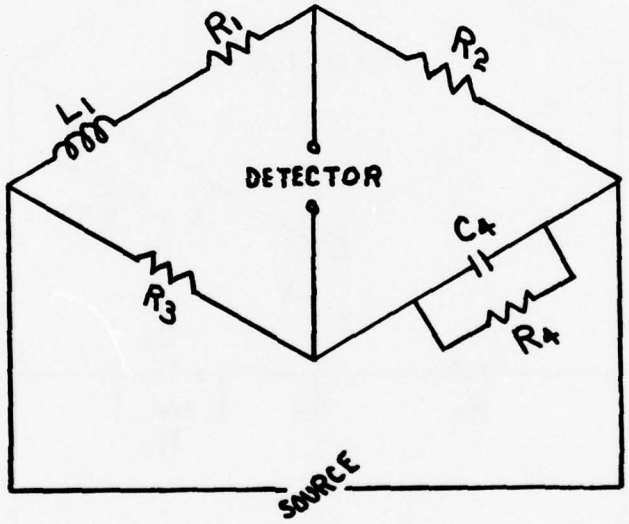

Figure 3. Maxwell bridge.

sensitivity with ease of operation since only variable resistors are needed thus avoiding the problems associated with variable inductors and capacitors. The balance conditions for this bridge are

[23] V. A. Brown and B. P. Ramsay, "The Maxwell Bridge at Low Frequencies," *Rev. Sci. Inst.*, Vol. 20, No. 4.

$$L_1 = C_4 R_2 R_3$$

and

$$R_1 = \frac{R_2 R_3}{R_4}$$

where L_1 and R_1 represent the inductance and resistance, respectively, of the leg of the bridge containing the sample coil.

10. Sensitivity and Wagner Grounding Device. An elaborate shielding scheme which utilized the Wagner grounding device to increase the sensitivity and the signal-to-noise ratio was used. This technique has the effect of keeping the potential of the detector at the potential of the surrounding walls, etc, and thus reduces the charges on this part of the bridge.

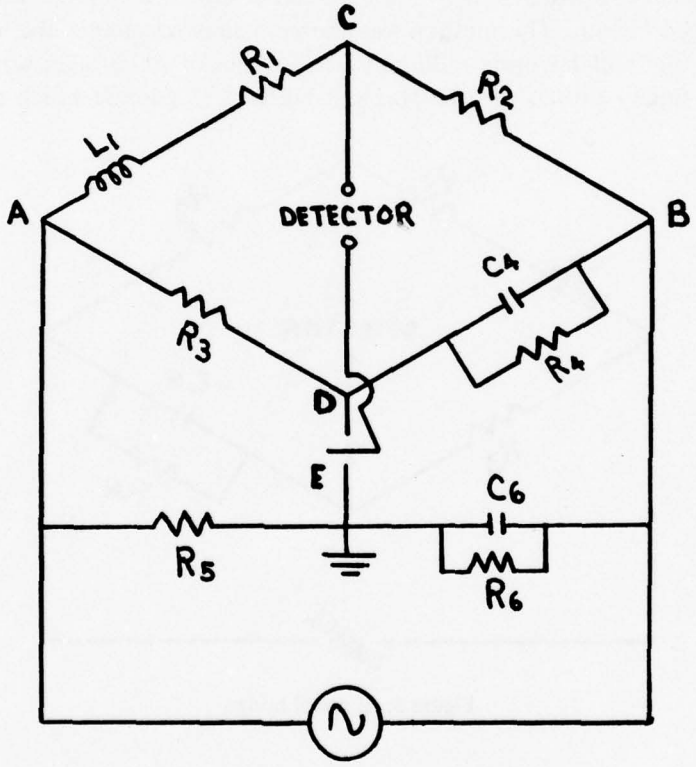

Figure 4. Maxwell bridge with Wagner grounding device.

The bridge balance condition $Z_1 Z_3 = Z_2 Z_4$ (Figure 4) merely implies that the branch points C, D are instantaneously at the same potential and not necessarily at 0 (ground) potential. Thus, current may still flow even when the balance condition

is fulfilled via the earth capacitances from C and D to the observer and nearby walls, tables, etc. To eliminate this effect, two auxiliary branches Z_5, Z_6 capable of balancing the impedances Z_1, Z_2 are joined as shown in the figure and earthed at their common point E. The earth capacitances from A and B to E merely shunt Z_5 Z_6. To eliminate the capacitances between C, D, and E, let the bridge be balanced as nearly as possible to the minimum deflection on the detector when joined between C and D. Now, transfer the detector into the auxiliary network between C and E balancing by means of Z_5 and Z_6. Now, C and E are nearly at the same potential, the latter being grounded. Reverting to the original bridge, balance can now be more nearly secured, and repetition of the process finally results in exact balance with C, D, and E at the same potential, namely, ground. A wiring diagram of the bridge and shielding circuit is shown in Figure 5.

Sensitivity tests were run on the measuring circuit using low-resistance copper coils similar to the coils to be tested. Using a PAR Lock-in Amplifier as the detector, the bridge was found to have a sensitivity of about 1×10^{-5} Ω. In actual operation, an oscilloscope, through Lissajous figures, is used as the detector for coarse balancing; and, then, the Lock-in Amplifier is used for fine balancing.

11. The Meaning of the Balance Condition. The objective of these bridge measurements is to determine actual power or resistive losses in superconducting coils. Thus, what is actually represented by the balance condition, $R_1 = \frac{R_2 R_3}{R_4}$? The four legs of the Maxwell bridge can be represented by impedance of the form

$$
\begin{aligned}
Z_1 &= X + iY \\
Z_2 &= R_2 \\
Z_3 &= R_3 \\
Z_4 &= \frac{R_4}{1 + i\omega C_4 R_4}
\end{aligned}
$$

where legs Z_2 and Z_3 are purely resistive while Z_1 is a combination of resistance and inductance including the test coil, and Z_4 is a combination of a resistor and capacitor. At balance, there is no potential across the detector and no current in the detector. Thus, current i_1 is common to Z_1 and Z_2, and i_2 is common to Z_3 and Z_4; so we have

$$
\begin{aligned}
i_1 Z_1 &= i_2 Z_3 \\
i_1 Z_2 &= i_2 Z_4 \\
Z_1 Z_4 &= Z_2 Z_3
\end{aligned}
$$

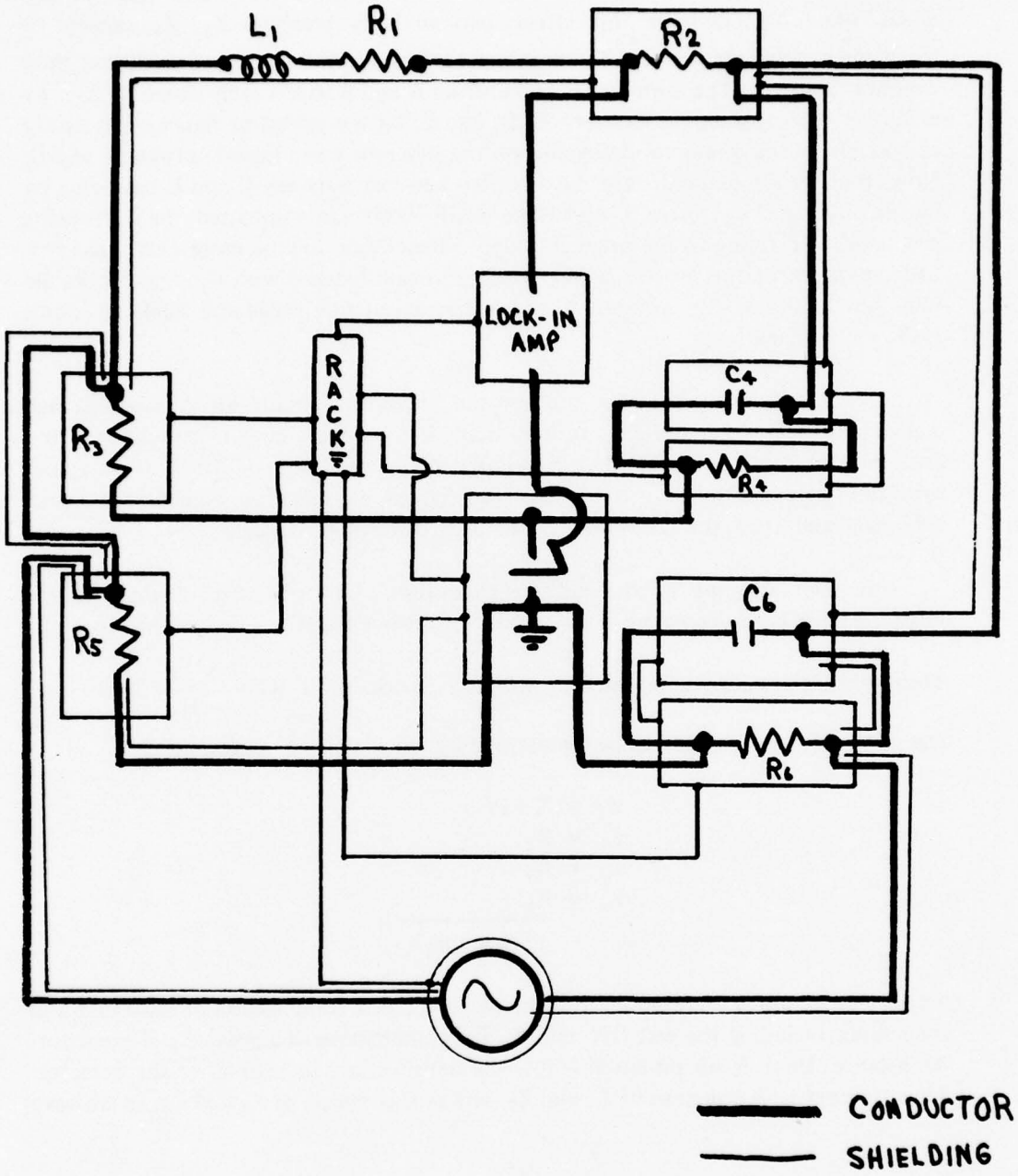

Figure 5. Wiring diagram.

which for the Maxwell bridge becomes

$$(X + iY) \frac{R_4}{1 + i\omega C_4 R_4} = R_2 R_3$$

or

$$R_2 R_3 (1 + i\omega C_4 R_4) = XR_4 + iYR_4.$$

Equating real parts gives

$$R_2 R_3 = XR_4$$

and

$$X = \frac{R_2 R_3}{R_4}$$

which says that $\frac{R_2 R_3}{R_4}$ is the real part of the impedance Z_1. Thus, we are measuring the effective resistance of the test coil which is precisely what we are interested in.

A complete electrical schematic of the bridge circuit with detectors, amplifiers, and oscillator is shown in Figure 6. The source of AC power is a variable frequency sine wave oscillator which is output to a differential amplifier where the signal is amplified and isolated without introducing a phase shift. An oscilloscope is used as the detector to coarsely balance the bridge, and a PAR Lock-in Amplifier provides null signal detection for the fine balancing required for the 10^{-5} Ω bridge sensitivity. The sample coil and leads are represented by R_1, L_1 while the bridge components R_2, R_3, R_4, R_5, C_4, and C_6 are General Radio decade resistors and capacitors. The leads connecting the sample coils with the remainder of the bridge circuit were made of Evenohm wire so that the lead resistance would be independent of the liquid helium level.

V. SAMPLES

12. Geometry and Construction. The wires were tested in the form of small, multilayer coils wound on coil forms as shown in Figure 7. These are small coils but are considerably larger than traditional small samples (lengths of wire of a few centimeters to a few meters in length) with the typical sample having wire lengths of 50 meters. All coils were wound on identical coil forms and in the same inductive manner so that the physical properties of the coils were as similar as possible.

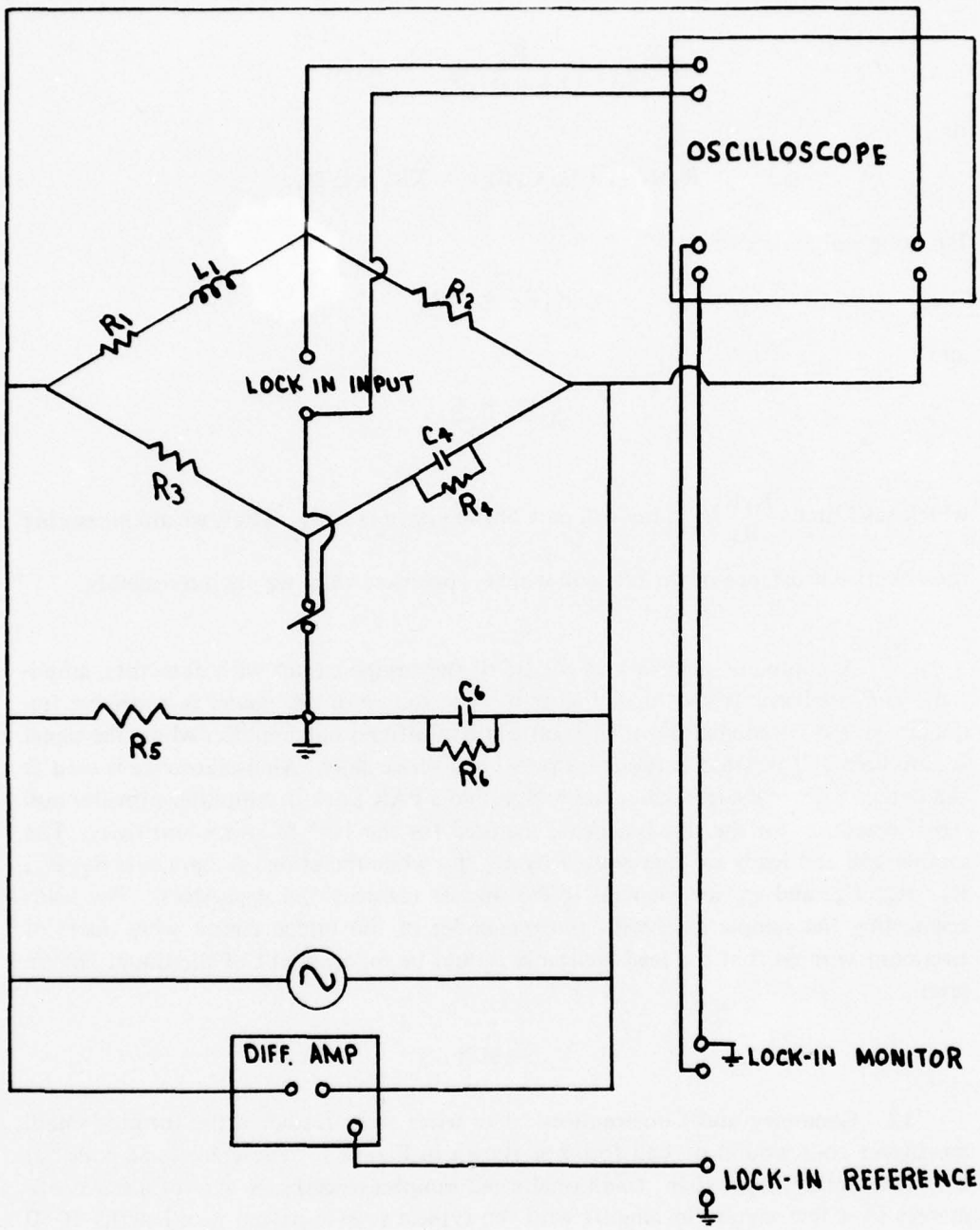

Figure 6. Schematic of measurement circuit.

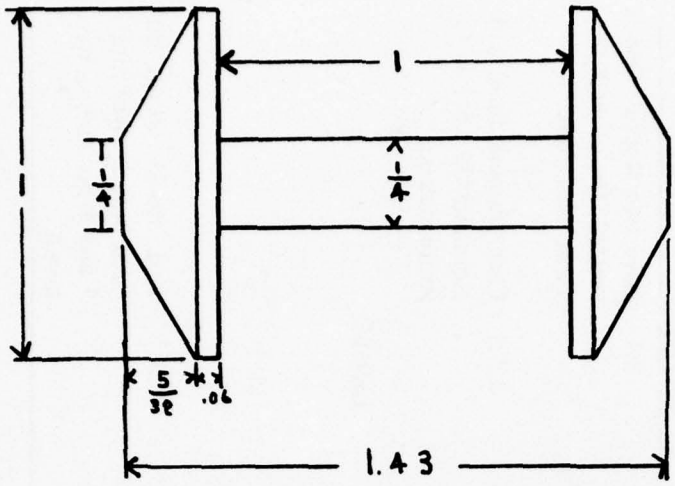

Figure 7. Sample coil form.

13. Conductor and Coil Characteristics. Tables 1 and 2 give the properties of the multifilament wires and the sample coils.

VI. EXPERIMENTAL METHOD AND DATA REDUCTION

14. Taking Data. Exploratory data runs indicated that the sensitivity of the apparatus was such that lead-resistance changes due to change in room temperature could be detected. To take this into account, the time was recorded each time a data point was taken. Due to the cycling of the air conditioner in the lab, the room temperature was closely correlated with the cycle time of the air conditioner so the time was used to make corrections with the cycle time of the air conditioner. This technique will be explained later but simply amounts to making linear interpolations between data points at different times.

The following procedure was used to insure that the resistive and inductive losses could be independently measured:

(1) Approximately balance bridge on 10- or 20-mV scale.

Table 1. Superconducting Materials

Material	Diameter Bare, In. (cm)	Fialment Diameter, In. (cm)	# Filaments	Twist Rate, Turns/In. (cm)	Ratio CU/S.C.	Miscellaneous Comments
Airco Kryoconductor NbTi	.015 (.038)	.0009 (.00228)	85	0 & 2 – (0 & .8)	2:1	Have two stocks. One is twisted, the other is not. Twist rate: 2/in.
Niomax TC	.016 (.040)	.00039 (.001)	1045	~ 7 (2.75)	1.5:1	Each filament lined with cupronickel; 1.5:1 is for entire matrix.
Supercon NbTi	.013 (.033)	.0005 (.00127)	400	5 (1.97)	1.69:1	
Niomax FM A61	.013 (.033)	.000906 (.023)	61	1 –	1.35:1	
Kryoconductor	.011 (.028)	.000394 (.001)	361	5 & 8 (2 & 3)	1.25:1	Two stocks which differed only in twist rate – 5 and 8 per inch – were tested.

Table 2. Superconducting Coils

No.	Symbol	Material	Wire Dia., In. (cm)	Total # Turns (# layers)	R, Ω (Room Temp.)	L, mH (Room Temp.)	Coil O.D., In. (cm)	Wire Length x 10^3 In. (cm)
1	⊙	Airco Kryoconductor – Untwisted	.019 (.048)	1089 (20)	10.3	5.65	.98 (2.49)	2.1 (5.3)
2	△	Airco Kryoconductor – Twisted	.019 (.048)	1015 (20)	10.5	4.28	.955 (2.43)	1.91 (4.85)
3	□	Niomax – TC Twisted 7 turns/in.	.017 (.043)	1215 (20)	15.6	6.55	.89 (2.26)	2.16 (5.5)
4	◇	Supercon Twisted	.014 (.0356)	1411 (22)	25.9	7.75	.825 (2.0955)	2.383 (6.05)
5	None	Niomax FM Twisted	.014 (.0356)	1279 –	17.4	5.82	.76 (1.93)	2.03 (5.15)
6	⨯	Kryoconductor 5 twists/in.	.013 (.033)	1278 –	26.8	5.18	.675 (1.71)	1.6 (4.1)
7	○	Kryoconductor 8 twists/in.	.013 (.033)	1274 –	27.6	5.225	.80 (2.032)	2.1 (5.34)

(2) Change the sensitivity setting on the Lock-in by two orders of magnitude to the 10-mV or higher scale.

(3) Introduce a large unbalance in the bridge by changing R_4 until a midscale reading is obtained on the Lock-in.

(4) Adjust the phase control until a maximum deflection is observed. The phase can be changed by 90° by the outer ring (quadrant switch) surrounding the phase shift. When this is done, the indicator should read 0, and when the quadrant switch is changed back to the 0° position the maximum deflection should be observed.

(5) Change R_4 back to its value preceding Step (3).

(6) Switch the sensitivity scale to the highest sensitivity possible for an on-scale reading. The bridge is now ready to be balanced.

As mentioned previously, the bridge is first balanced using the oscilloscope as the detector. Then, a more sensitive balance is obtained by using the Lock-in Amplifier as the detector; this allows the bridge to be balanced within a few tenths of a millivolt of zero.

15. Anomalous Resistance Effect. The reduction of data from the first two samples indicated an unexpected and initially unexplained behavior. It was anticipated that the resistance would increase continuously with frequency from 0 Hz since the eddy-current losses increase with the square of the frequency. However, the initial data demonstrated a behavior as shown in Figure 8 where we see that between 5 and 350 Hz the resistance decreases with increasing frequency reaching a minimum at about 350 Hz at which point it begins a rapid increase with frequency.

Initially, this behavior was attributed to frequency response[24] [25] of the bridge associated with nonideal components such as inherent inductance and capacitance of the decade resistors and the capacitance of the test coil. However, a number of complicated calculations were performed on the bridge circuitry, and these seemed to eliminate any nonideal characteristics of the arms of the bridge as the source of the anomaly. A separate test was run on a typical superconducting test coil to determine the self capacitance of the coil. The resonant frequency of the coil was determined by using the circuit shown in Figure 9 where L_1, R_1, and C_1 represent the inductance, resistance, and capacitance, respectively, associated with the test coil. The resistance, R_1, represents the resistance of the coil and the leads, and the value of L_1 has been

[24] V. A. Brown and B. P. Ramsay, "The Maxwell Bridge at Low Frequencies," *Rev. Sci. Inst.*, Vol. 20, No. 4.

[25] B. Hague, "Alternating Current Bridge Methods," as revised by T. R. Foord and S. T. Machay, 1971, Pitnum Press.

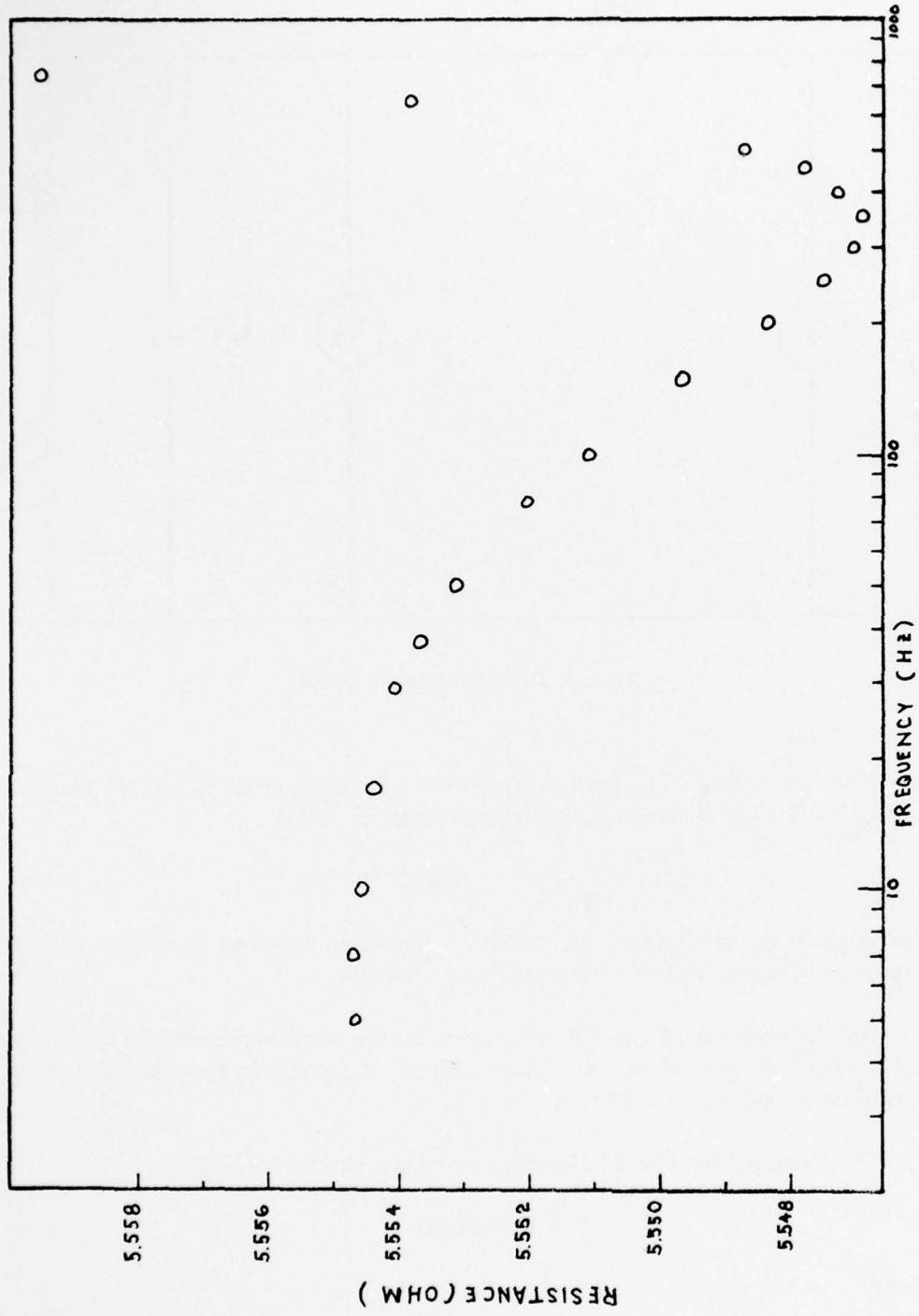

Figure 8. Anomalous resistance effect.

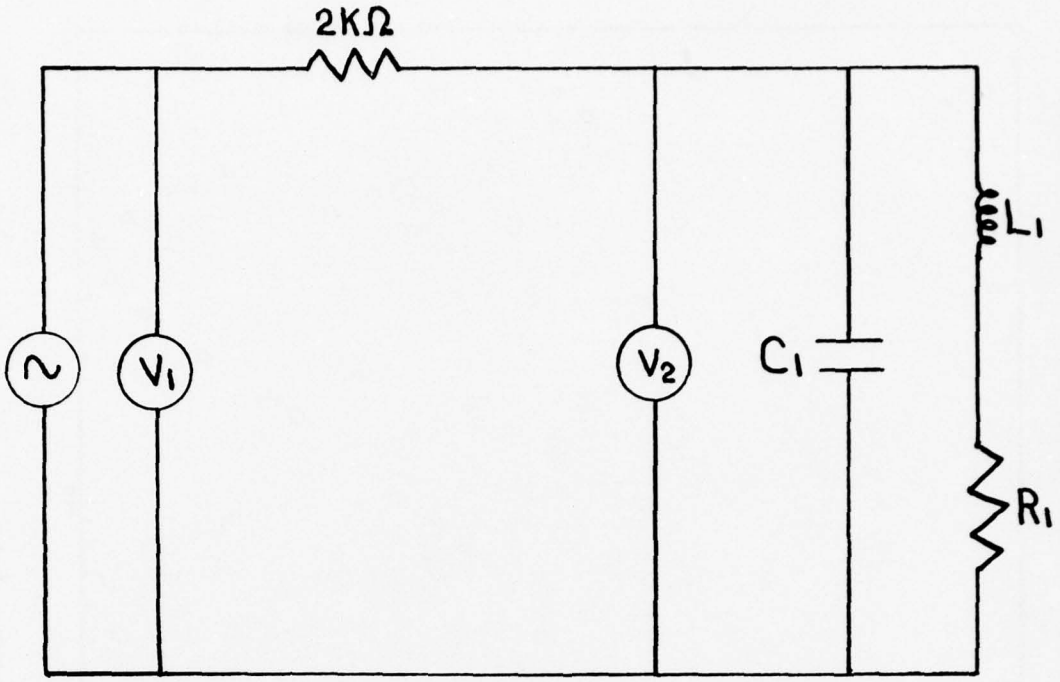

Figure 9. Resonant frequency circuit.

previously determined. The resonant frequency was found to be 1.75×10^5 Hz, and with $L_1 = 3.3 \times 10^{-3}$ H, the inherent capacitance of the coil is

$$C_1 = \frac{1}{\omega_o^2 L} = 2.52 \times 10^{-10} \text{ F.}$$

This value of capacitance is several orders of magnitude too small to account for the anomalous behavior in the 0 – 1000 Hz frequency range.

16. Explanation of the Effect. The following derivation considers the effect that a change in inductance during each cycle of AC current in the superconducting coil has on the balance of the bridge.

Consider the sinusoidal driving current supplied by the oscillator

$$I = I_o \text{ Sin } (\omega t) \qquad (1)$$

where

I_o = peak current.

Figure 10 shows the actual sinusoidal variation of current in the coil. The solid curve of Figure 10 represents the change in inductance based on qualitative arguments (to be given) while the broken curve represents a more mathematically manageable situation. The relative magnitudes of the curves in Figure 10 are exaggerated because the "bias" inductance, L_o, is very large compared to the amplitude of the sine wave variation since we are dealing with very low currents. In fact, the currents are so low that $H < H_{c1}$, and only slight penetration is assumed to be caused by the AC current in the coil.

A qualitative argument will now be presented to justify the assumption represented in Figure 10. The basic assumption is that some flux realignment occurs as the sinusoidal voltage varies. One complete cycle is broken into four regions:

(1) As the voltage increases from 0 to its peak value, the inductance of the coil increases (due to increasing flux penetration) from its "bias" value, L_o, to some maximum value because at V_{max}, maximum flux penetration occurs and thus L is maximum.

(2) As the voltage decreases from its peak value back to zero, the flux penetration goes from maximum to minimum, thus L goes from L_{max} to L_o.

(3) As the voltage decreases from 0 to $-V_{max}$, the inductance increases from L_o to L_{max}. This occurs because the flux penetration does not depend on the sign of V (actually H) but only on its magnitude.

(4) For the same reasons as in (2), when the voltage goes from $-V_{max}$ to 0, the inductance goes from L_{max} to L_o.

This argument explains the reasoning behind the solid curve of Figure 10, but the broken curve is used in the analysis as an approximation which is easier to handle mathematically. Thus, the inductance change is approximated as a sine wave of frequency 2 ωt.

So, for the coil inductance, we have

$$L \sim L_o + L' I$$

where L' is the magnitude of the change of L. In the full, sine-wave approximation, we can write

$$L \sim L_o + L' \sin (2 \omega t). \qquad (2)$$

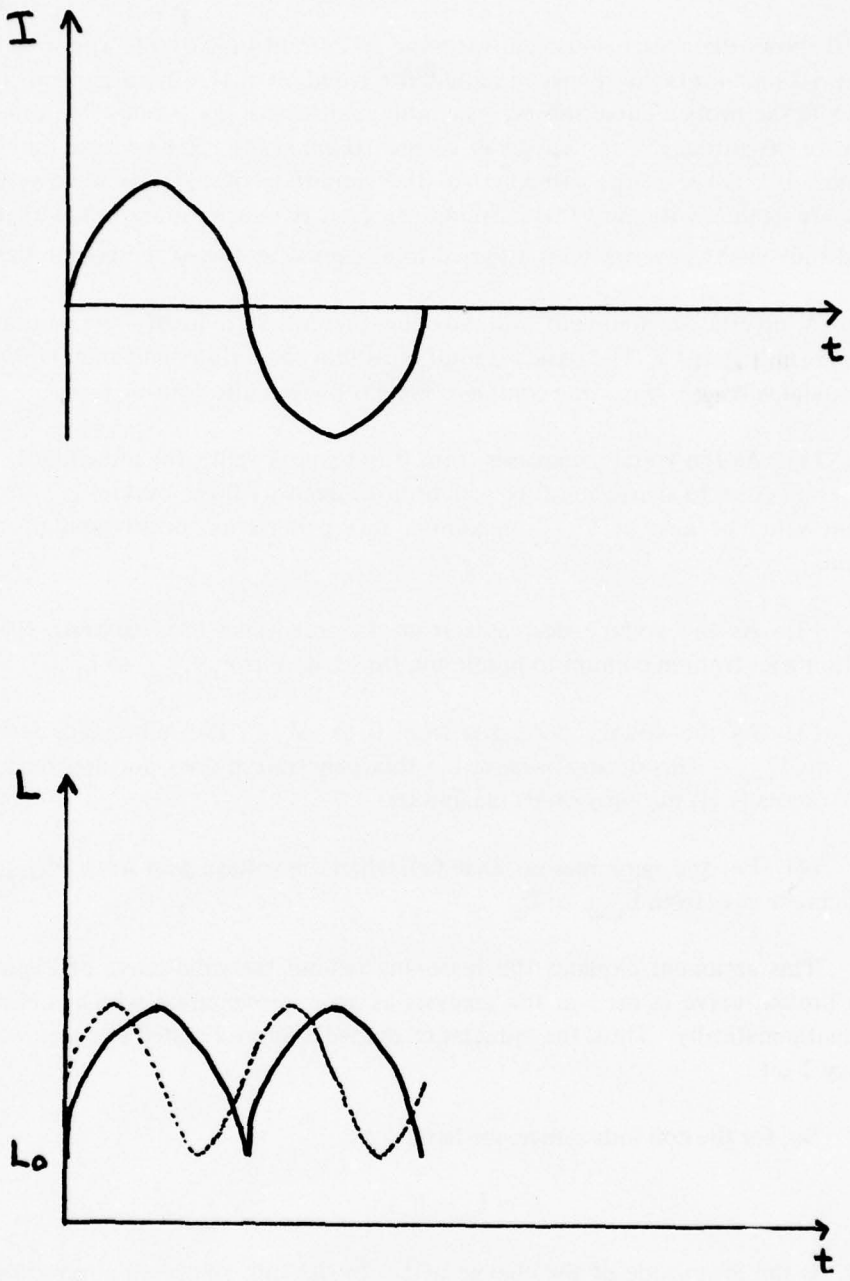

Figure 10. Current and inductance variation.

Now, the change of L with time is

$$\frac{dL}{dt} = 2\,\omega L' \cos(2\,\omega t). \tag{3}$$

From E & M theory, the energy stored in a coil is

$$E = \tfrac{1}{2} LI^2$$

so the power is

$$\frac{dE}{dt} = LI\,\frac{dI}{dt} + \tfrac{1}{2} I^2\,\frac{dL}{dt} = VI$$

$$\therefore V = L\,\frac{dI}{dt} + \tfrac{1}{2} I\,\frac{dL}{dt}\,. \tag{4}$$

Substituting the derivative of (1) and (3) into (4) gives

$$V = LI_o\,\omega \cos \omega t + \omega\, IL' \cos 2\,\omega t$$

$$= L_o I_o\,\omega \cos \omega t + L' I_o\,\omega \sin 2\,\omega t \cos \omega t + \omega\, I_o L' \sin \omega t \cos 2\,\omega t. \tag{5}$$

At this point, (5) should be put into the response equation for a lock-in amplifier, but first we take the voltage and divide it into two components – one in phase with the current and one at $\pi/2$ with the current.

In phase

From (5):

$\omega t = \pi/2$

$V = \omega I_o L'$

$\therefore Z_{o=o} = -\omega L'$ in phase with I

$\pi/2$ out of phase

$\omega t = o$

$V = L_o I_o \omega$

$\therefore Z = \omega L_o$ $\pi/2$ out of phase with I

$\theta = \pi/2$

So, the bridge balance equation becomes

$$\mathrm{Re}(Z_1) = \frac{R_2 R_3}{R_4} = R_1 + R_L - \omega L' \tag{6}$$

where

R_1 = Coil resistance

R_L = Lead resistance

and

$$\mathrm{Im}\,(Z_1) = C_4 R_2 R_3 = \omega L_o$$

and (6) gives

$$R_1 - \omega L' = \frac{R_2 R_3}{R_4} - R_L \tag{7}$$

now

$$R_1 = \alpha \omega^2$$

where α is just a constant of proportionality. Substituting this into (7) and dividing by ω gives

$$\omega - L' = \frac{\frac{R_2 R_3}{R_4} - R_1}{\omega} . \tag{8}$$

If the right side of this equation is plotted as a function of ω, the Y-axis intercept should give L'. If this is a reasonable value, $L' \ll L_o = 3 \times 10^{-3}$ H and, in fact, L' has a typical value of 10^{-5} H.

This theory can be used successfully to explain the anomalous behavior described in the previous sections, and it is this method which will be used to reduce the resistance data.

17. Data Reduction. The basic reduction of the direct-resistance measurements consists of compensating for changes in room temperature and for the inductance changes described in para. 16. A frequency of 100 Hz is used as the base for the room temperature compensation. The data-reduction scheme is given below:

(1) Plot $\left[\frac{R_2 R_3}{R_4}\right]_{\text{all t}}^{f = 100}$ vs time.

(2) Adjust each $\left[\frac{R_2 R_3}{R_4}\right]_{t}^{f = x}$ reading to one time $t = t_o$ by using

$$\left[\frac{R_2 R_3}{R_4}\right]_{t = t_o}^{f = x} = \left[\frac{R_2 R_3}{R_4}\right]_{t}^{f = x} - \left[\frac{R_2 R_3}{R_4}\right]_{t}^{f = 100} + \left[\frac{R_2 R_3}{R_4}\right]_{t_o}^{f = 100}$$

(3) Plot $\left[\frac{R_2 R_3}{R_4}\right]_{t_o}^{f = x}$ vs frequency. Extrapolate to f = o to get R_o.

(4) Calculate $R_1 = \omega L' = \left[\frac{R_2 R_3}{R_4}\right]_{t_o}^{f=x} - R_o$ for each frequency.

(5) Calculate $\frac{R_1 - \omega L'}{\omega}$ for each frequency.

(6) Plot $\frac{R_1 - \omega L'}{\omega}$ vs ω on cartesian coordinates. Then, plot L′ as the Y-intercept and α as the slope.

(7) Use L′ determined above to calculate R_1 which is the coil resistance

$$R_1 = \left[\frac{R_2 R_3}{R_4}\right]_{t}^{f=x} - R_o + \omega L'.$$

(8) Plot R_1 vs f.

Several computer programs are used to perform this scheme, and listings of these programs are included as Appendices B and C.

VII. DATA ANALYSIS AND RESULTS

18. Results. The method described in paragraph 16 is quite successful in accounting for the seemingly anomalous behavior of the effective resistance as a function of frequency. This is demonstrated in Figure 11 in which the data is compared with theoretical calculations based on the method described in paragraph 16. This graph is typical of the samples and shows excellent agreement between experimental results and theoretical calculations.

Computer calculations were made to determine the magnetic-field profiles of the coils; typically, the maximum field obtained in the test coils was approximately .005 T indicating operation below H_{c1}. This means there was no penetration of the magnetic field into the superconductor; therefore, hysteresis losses would be negligible, and eddy currents in the stabilizer were expected to be the dominant loss mechanism. Some data was taken with an externally applied field; however, much of this data was unreliable due to electromagnetic instabilities caused by the mutual inductance between the sample and field coils.

The plot of Figure 12 shows the measured resistance of each sample as a function of frequency and shows some unexpected results. These resistances are converted to power losses in Figure 13, and finally the normalized power losses as a function of current are plotted in Figure 14. Since the dominant loss mechanism is thought

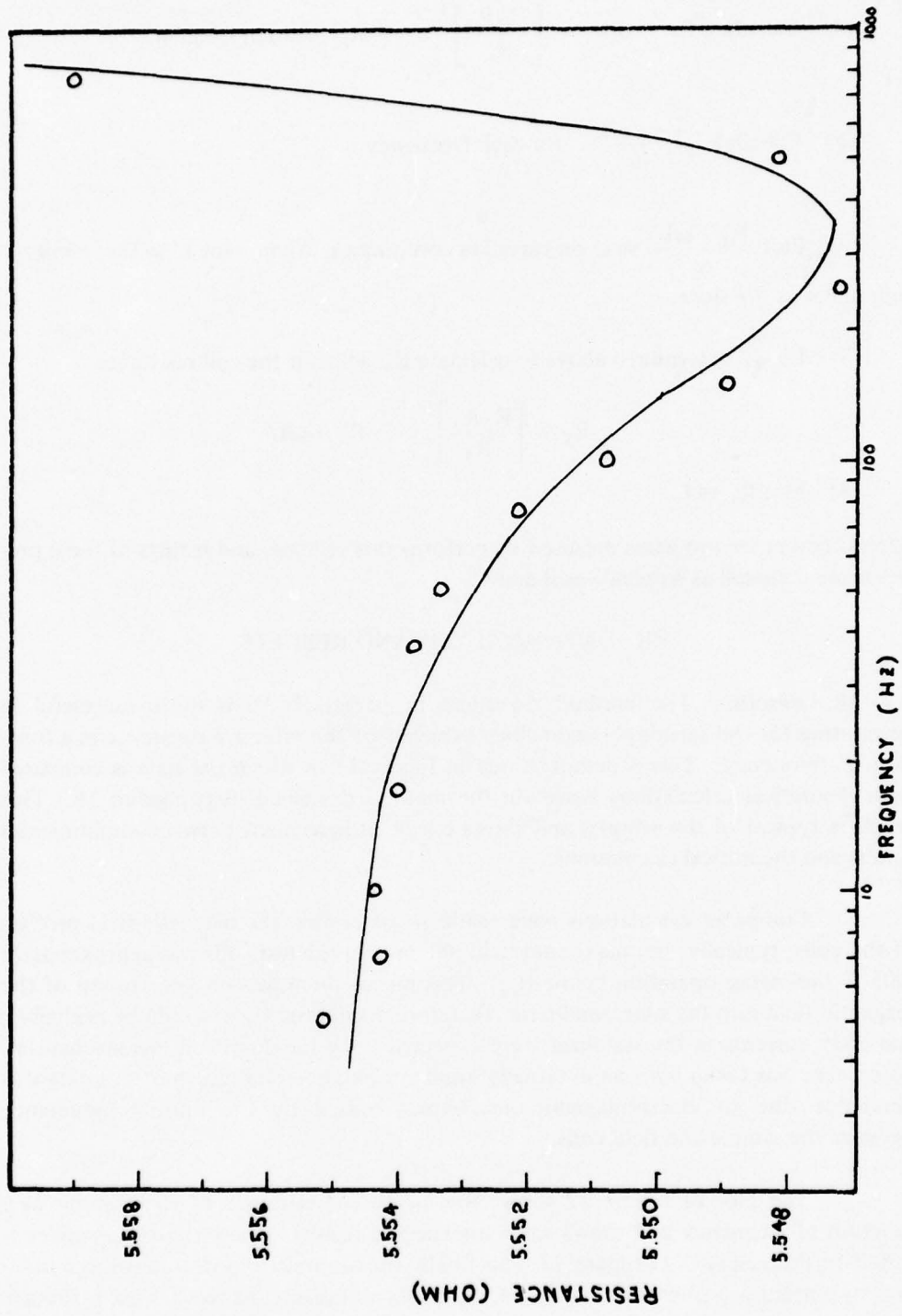

Figure 11. Comparison of data with theory of anomalous resistance effect.

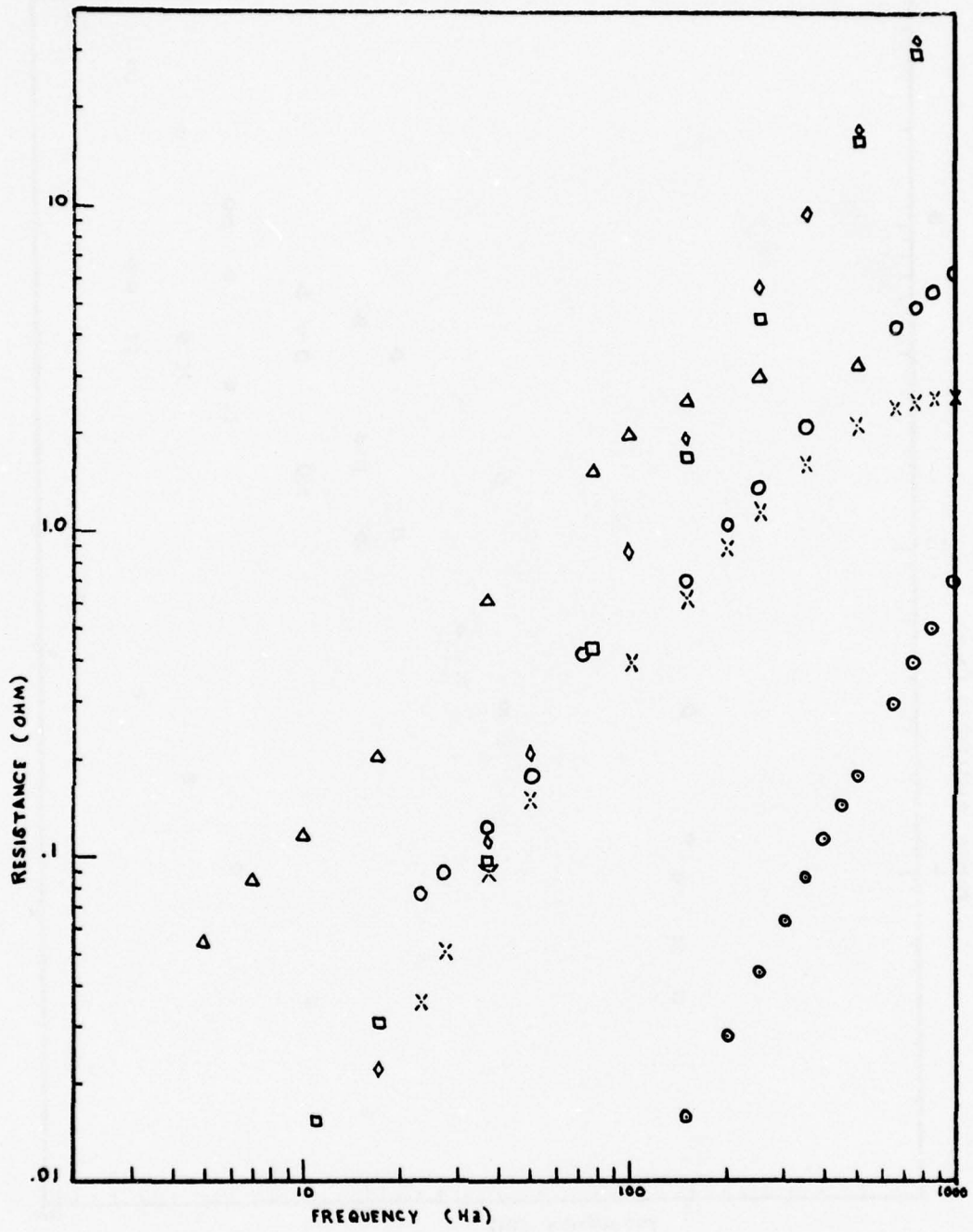

Figure 12. Resistance of samples. (Symbols defined in Table 2.)

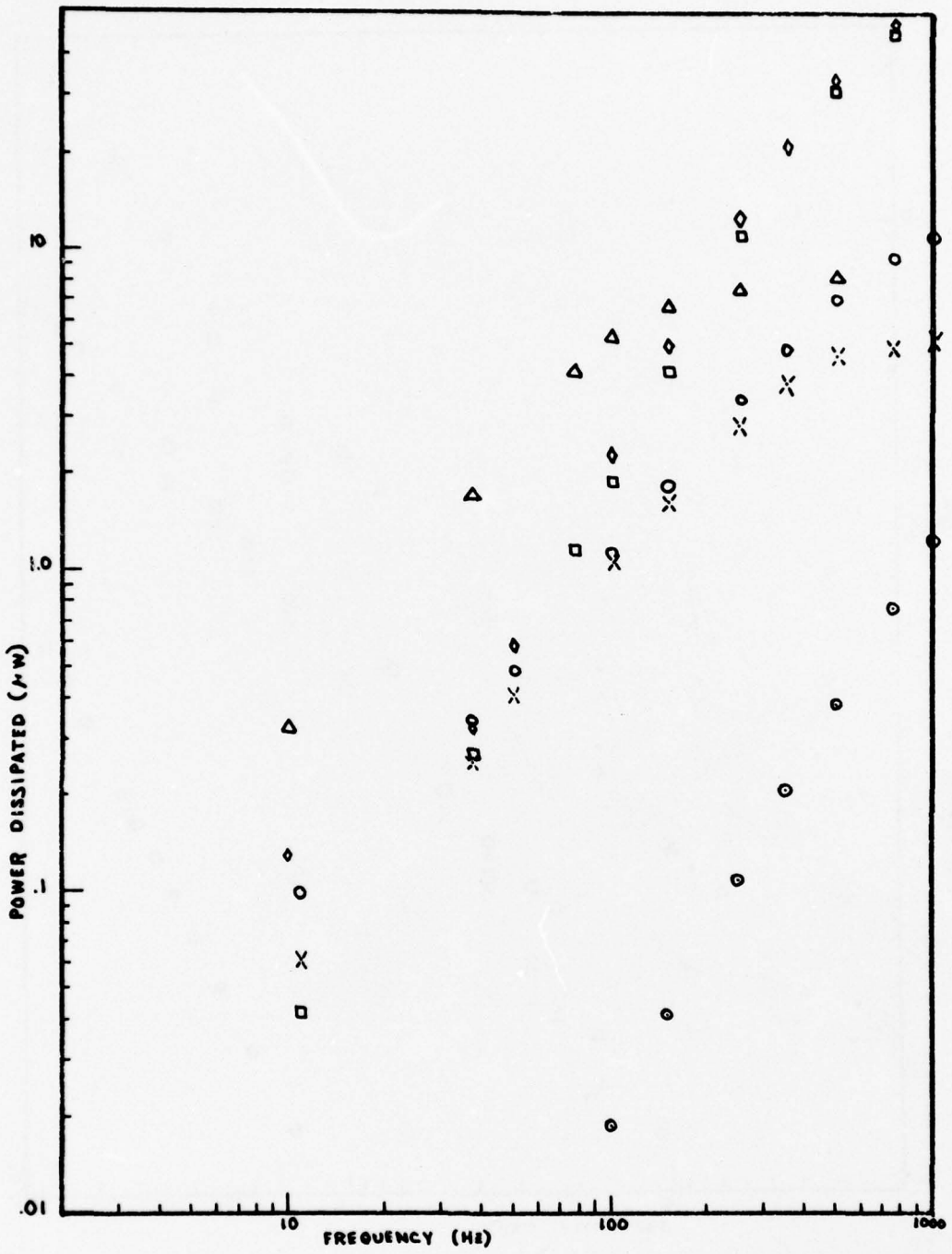

Figure 13. Power losses of samples. (Symbols defined in Table 2.)

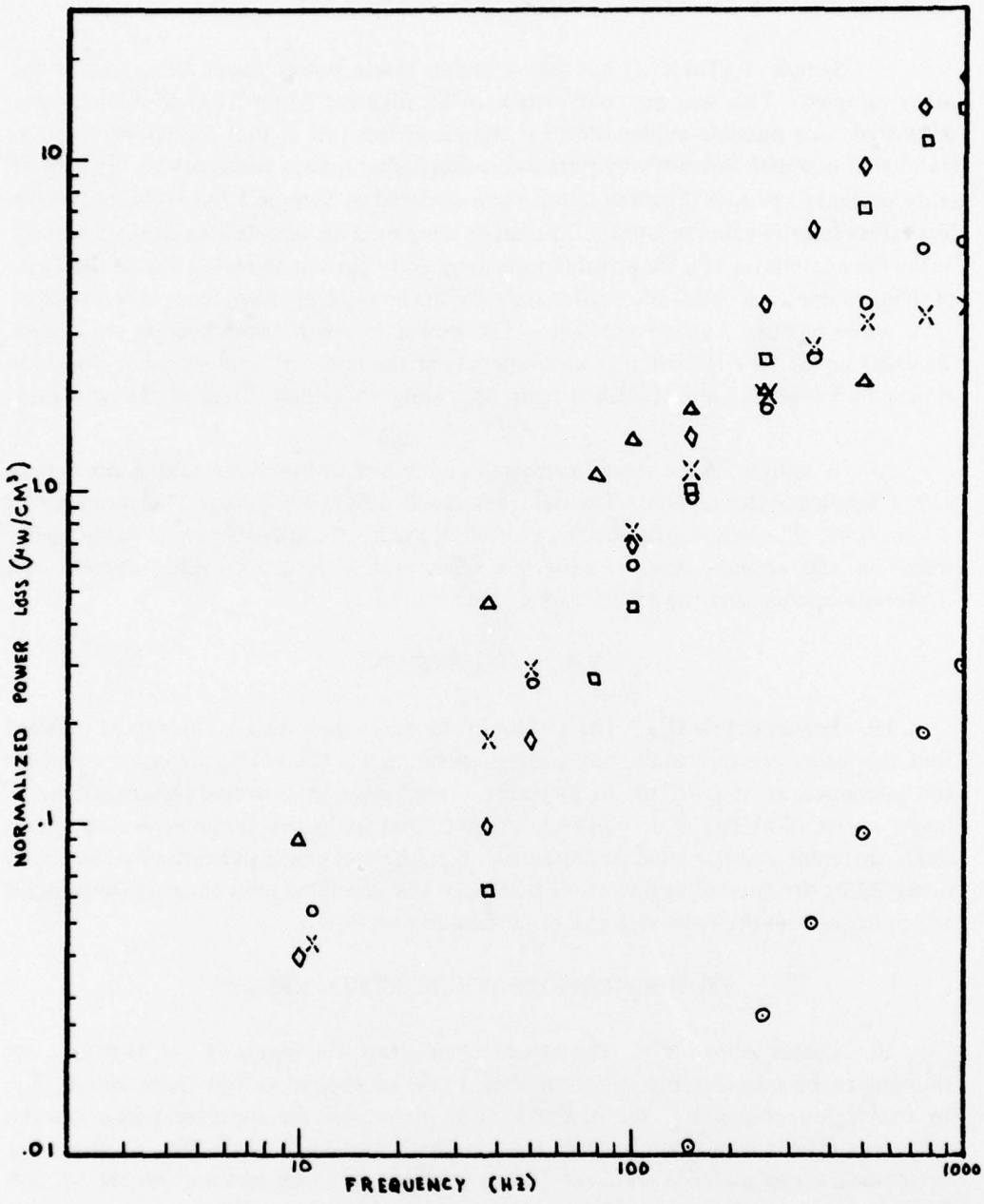

Figure 14. Normalized power losses. (Symbols defined in Table 2.)

to be eddy currents in the copper stabilizer, the normalization procedure is to divide the power losses by the volume of copper in each sample coil.

Sample 1 (Table 2) had considerably lower power losses than any of the other samples. This was an "old" stock of 85 filament Airco NbTi wire which was untwisted; one possible explanation for the lower loss rate is that the copper used as stabilizing material was not very pure indicating higher matrix resistivity to the flow of eddy currents. Sample 2 which is the same material as Sample 1 but is twisted shows loss rates closer in value to those of the other samples. This sample also shows a "knee" in the curve at about 100 Hz possibly indicating eddy current shielding due to the twist of 2/in. Samples 6 and 7 also differ only by the amount of twist; Sample 6 is twisted 5/in. while Sample 7 is twisted 8/in. The power losses of these samples are almost identical up to 500 Hz where a knee appears in the curve of Sample 6 but does not appear in Sample 7 until 1000 Hz, again indicating a shielding effect of the twist rate.

A sample of the Airco untwisted conductor was used for taking loss data in a .6 T applied, external field. The field was supplied by a 3.5 T Nb_3Sn solenoid with a 1.5-in. bore. The results of this data, plotted in Figure 15, indicate considerably higher losses in the applied field as expected since in this case both eddy current and hysteresis mechanisms contribute to the losses.

VIII. CONCLUSIONS

19. Losses Below H_{c1}. The results of the study described in this report indicate that the losses in superconducting coils in applied fields below H_{c1} are not reduced by the introduction of twist to the filaments. This was demonstrated in measurements made up to 1000 Hz; it is, however, possible that at higher frequencies and higher fields different results could be obtained. Such behavior was indicated by the knees observed in the twisted samples which showed that shielding may occur at frequencies which depend on the twist rate and other sample properties.

IX. SUGGESTIONS FOR FURTHER STUDY

20. Losses Above H_{c1}. The loss mechanisms in the region $H_{c1} < H < H_{c2}$ are thought to be considerably different than those in applied or self fields below H_{c1}. In the region above H_{c1}, the magnetic field penetrates the superconductor causing hysteresis effects which can become the dominant loss mechanism. Such a study has been undertaken under Work Unit 109 as well as studies on losses at 60 Hz AC and variable frequency DC up to 10 Hz. Although there is an abundance of transient-loss data on small, non-inductively-wound coils, there is currently little data on multilayer, inductive coils which operate under large self-fields. The data obtained in this effort will also be used to verify models developed as explained in Appendix A.

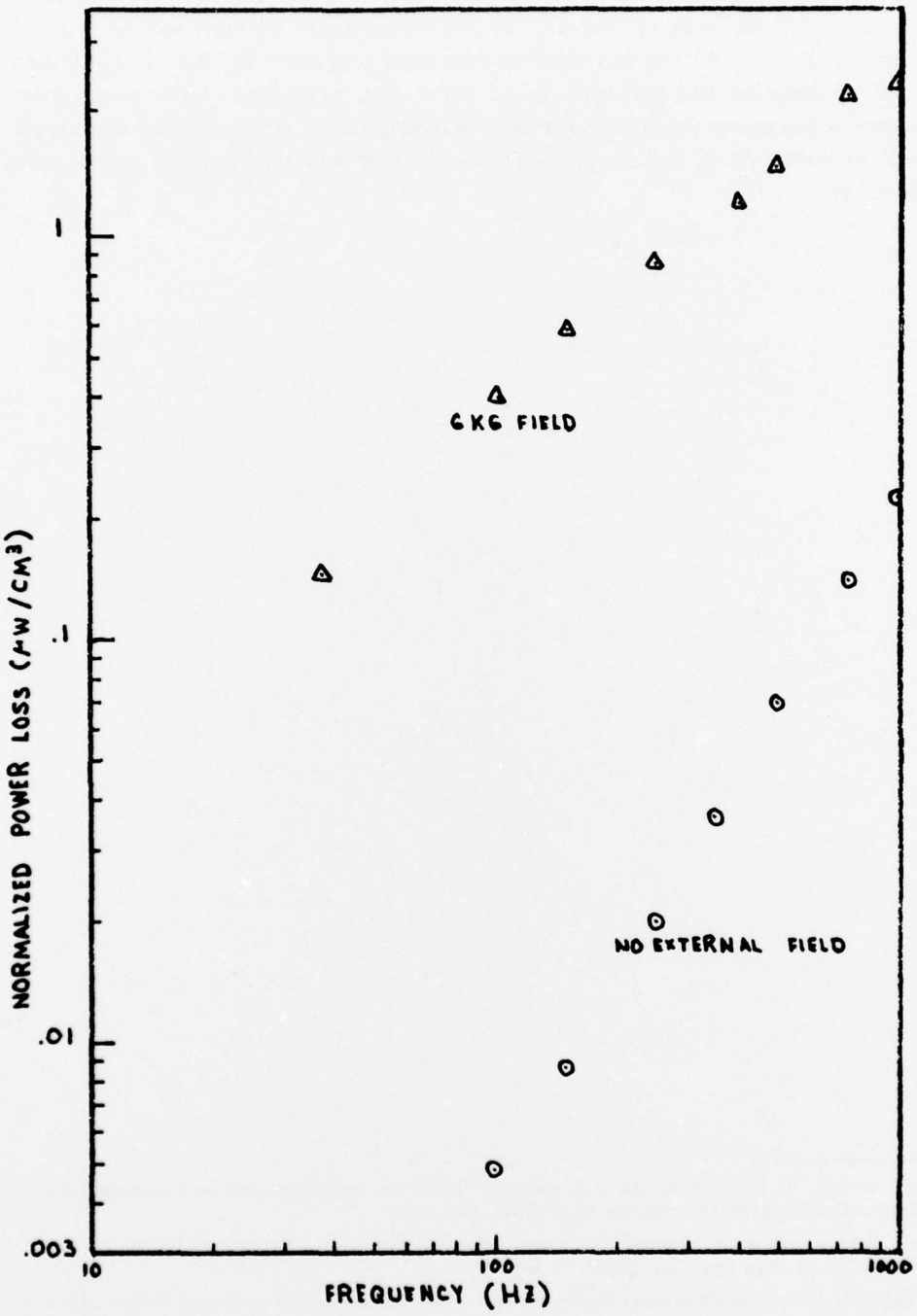

Figure 15. Losses with and without external field.

Multifilamentary wires of Nb_3Sn have become commercially available,[26 – 29] but there is little data on the DC or AC performance of coils wound from these materials. Because Nb_3Sn has superior high-field properties to NbTi, it would be very useful to examine the performance of these new materials. Since most potential military applications would call for large transient fields, an experimental study of the transient losses would make a general scientific and military contribution of considerable value.

---

[26] M. Suenaga, W. B. Sampson, and T. S. Luhman, "Effects of Heat Treatments on Superconducting Critical Current Densities of Multifilamentary Nb_3Sn Wires, *BNL 17425.*

[27] M. Suenaga and W. B. Sampson, "Superconducting Properties of Multifilamentary Nb_3Sn Made by a New Process," *Appl. Phys. Lett.*, Vol. 20, No. 11, June 1972.

[28] "Industrial News: Multifilamentary Nb_3Sn is Now Available Commercially," *Cryogenics*, February 1975.

[29] C. E. Oberly, M. C. Ohmer, and H. L. Gegel, "Properties of Multifilament Nb_3Sn in Useful Conductor Configurations for Superconducting Rotating Machines," **Private communication.**

APPENDIX A

Reprinted from: ADVANCES IN CRYOGENIC ENGINEERING, VOL. 19
Edited by K. D. Timmerhaus
Book available from: Plenum Publishing Corporation
227 West 17th Street, New York, New York 10011

E—2

THE APPLICATION OF LOSS MODELS TO SUPERCONDUCTING SOLENOIDS

J. T. Broach and W. D. Lee

U. S. Army Mobility Equipment Research and Development Center
Ft. Belvoir, Virginia

INTRODUCTION

The use of inductors, both cryogenic and superconductive, for the storage of energy in pulsed power systems of various types has recently attracted considerable attention. The storage element is usually operated in a pool of liquid cryogen but for certain applications, integrated refrigeration using helium gas is desirable. In either case, an estimate of the losses generated during transients is an essential part of the design. The principal loss mechanisms in the superconducting case are eddy currents in the stabilizer and hysteresis in the superconductor, both of which depend upon the magnitude and frequency of the transient field. This presentation presents the results of an application of loss models to a particular configuration of multifilament superconductor. The eddy current loss model is compared separately to loss measurements made on a coil wound from commercial copper wire. Losses calculated using a simple linear model of the field in the winding are compared with those obtained from a more sophisticated calculation using digital computer techniques.

EDDY CURRENT LOSSES

The power losses due to eddy currents caused by a time-varying self-field in a normally conducting solenoid will first be calculated. The magnetic field is assumed to be axial and the eddy currents are assumed to flow in circular paths within the wire.

Applying the integral form of Faraday's law to the circular geometry of an eddy current with a maximum radius r_m, we obtain the electric field driving the eddy currents

$$E = \tfrac{1}{2} r_m \dot{B} \tag{1}$$

From Ohm's law, the power density can be written, using (1), as

$$\dot{q} = (r_m^2/4\rho)\dot{B}^2 \tag{2}$$

Working in spherical coordinates, taking the field along the $\theta = 0$ axis so that $r_m = r \sin\theta$,

$$\dot{q} = [(r^2 \sin^2\theta)/4\rho]\dot{B}^2 \tag{3}$$

Integrating to get the average loss per unit volume

$$\frac{\dot{Q}}{V} = \frac{\int_0^{\pi}\int_0^{2\pi}\int_0^{r_w} [\dot{B}^2 r^2 (\sin^2 \theta)/4\rho]\, dV}{4\pi r_w^{\,3}/3} \tag{4}$$

results in

$$\dot{Q}/V = \dot{B}^2 r_w^{\,2}/10\rho \tag{5}$$

Assuming a sinusoidal transport current, this becomes

$$\dot{Q}/V = B_m^{\,2}\omega^2 r_w^{\,2}/20\rho \tag{6}$$

To check this model, measurements of the effective resistance of a copper coil were taken at various frequencies with a Maxwell bridge [1]. To obtain the frequency dependence, the dc resistance was subtracted from the measured value at each frequency. The measured resistance was converted to power loss by using I^2R_{eff}. Values of the power loss obtained in this way are compared in Fig. 1 with the results calculated from (6). The value of resistivity, 1.6×10^{-10} Ω-m, used in the loss calculation was determined experimentally at 4.2 K. An expression for B which varies linearly across the winding was used. The departure of the measured values from a straight line at the higher frequencies is due to the fact that the experiment was run at constant voltage across the bridge. As frequency is increased, the impedance of the coil increases; therefore this arm draws less current and the I^2R decreases below the expected value.

In order to derive an expression for eddy current losses in the copper stabilizer of multifilament superconducting wires, the method used in the solid copper wire

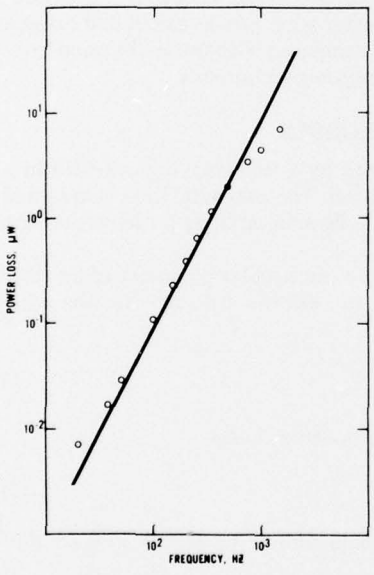

Fig. 1. Power loss vs. frequency for copper coil at 4.2 K.

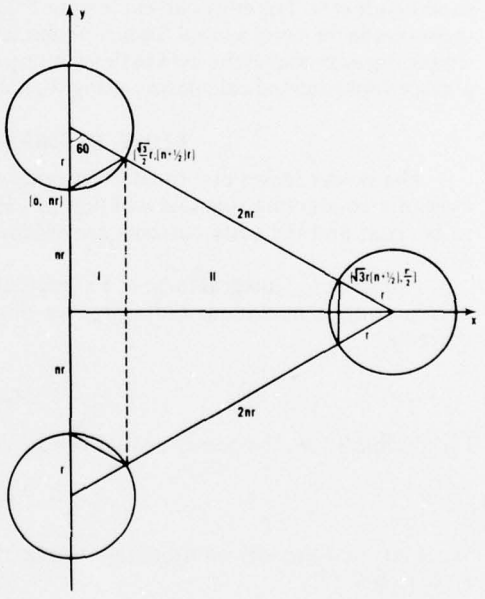

Fig. 2. "Unit cell" for multifilament conductor.

derivation was adapted to a geometry in which the filaments are distributed throughout the wire cross section. The eddy currents are confined to the regions of copper between the filaments. Considering a cross section of the composite, we assume a "unit cell" defined by superconducting filaments of circular cross section (see Fig. 2). The composite is taken to consist of "hcp" cylinders which represent the filaments; the spacing of the filaments is taken as a multiple of the filament radius, allowing application to a variety of conductors. The integration of the eddy current paths was taken in the regions between the filaments so that the power loss per unit volume of copper was calculated. The spacing of the unit cell was estimated from the number of filaments, the copper-to-superconductor ratio, and measurement of photomicrographs. Applying (3) to the geometry of Fig. 2 and integrating yields the loss per unit volume

$$\frac{\dot{Q}}{V} = \frac{2\pi \dot{B}^2}{V\rho} \int_0^x \frac{r_m^4}{4}\, dx' \tag{7}$$

Referring to Fig. 2, r_m is equal to one-half the distance in the y direction between the outer boundaries of the unit cell taken in such a way as to exclude the region occupied by the superconductor filaments. The expression obtained for a single "unit cell" is

$$\frac{\dot{Q}}{V} = \frac{\dot{B}^2 d^2}{8\rho}\left(\frac{n^5}{5} + n^4 + n^3 + \frac{n^2}{2} + \frac{n}{8} + \frac{1}{160}\right) \Big/ \left(\frac{n^3}{3} + n^2 + \frac{n}{2} + \frac{1}{24}\right) \tag{8}$$

HYSTERESIS LOSSES

The hysteresis losses in a solenoid wound from composite superconductor can be estimated using a model due to Bean [2,3]. A long solenoid can be approximated as a multilayer scroll wound from a sheet of superconducting material. The local power dissipation per unit volume derived by Bean [3] is given as

$$\dot{q} = \frac{\lambda J_c d' B_0}{4\tau}\left(\frac{a_2 - r}{a_2 - a_1}\right) \tag{9}$$

This expression assumes a simple linear variation of field in the winding as a function of r and assumes no variation with z (displacement parallel to the axis). A coil design based on NIOMAX TC* composed of 101 turns of a single layer of 144-strand braid having $a_1 = 0.194$ m, $a_2 = 0.202$ m, $l = 0.792$ m, $\lambda = 0.3$, and designed for $B_0 = 1.4$ T and an inductance of 2×10^{-3} H with 10^5 J stored energy resulted in calculated losses of 1.24 J/cycle.

For many solenoid configurations, the simple linear field profile assumed above is a good representation. To determine the error which might be introduced in design estimates through the use of (9), a more refined estimate of the field profile for the case described was made with the aid of a digital computer. The algorithm was based on the superposition of field contributions due to a finite number of current loops. The field was found to be approximately linear with r near the midplane with the field reversing at a point near the outer winding edge. Near the end of the coil, the field was proportional to r^2. To simplify the estimate based on (9), the coil was divided into regions and the field profile in a region was fitted to a simple algebraic expression. Calculated hysteresis losses based on this method were found to be approximately 5% lower than the previous estimate.

* Imperial Metal Industries, Ltd., Birmingham, United Kingdom.

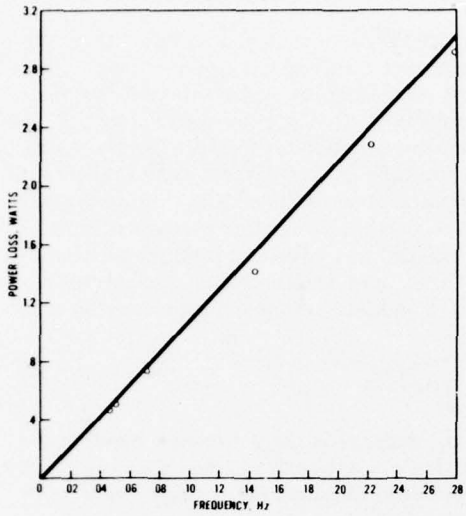

Fig. 3. Power loss vs. frequency for a small solenoid. Circles are the experimentally measured values and the line represents the calculated loss.

The method described above has been compared to calorimetric measurements of solenoid losses made at low frequencies by Jüngst [4]. Eddy current losses were negligible at these frequencies. The results are shown in Fig. 3. There is fair agreement between the calculated and experimental results in this frequency range, although the slope of the curve differs from that of a curve drawn through the data points. The solenoid upon which the calculation is based has an ID of 0.024 m, an OD of 0.065 m, and a length of 0.053 m. The conductor has a diameter of 0.0004 m and is composed of 61 35-μm Nb–Ti filaments with a twist rate of four turns/in. The copper-to-superconductor ratio is 1.4:1. Central field is 5.2 T at 46.9 A.

NOTATION

a_1 = inner winding radius
a_2 = outer winding radius
B = magnetic flux density
B_m = sinusoidal peak flux density
B_0 = central field of solenoid
d = superconductor filament diameter
E = electric field strength
I = rms transport current
J_c = superconductor critical current density
l = winding length
n = scale factor (not necessarily integral) for filament radius specifying spacing of composite
Q = power
q = power density
r = radial position
R_{eff} = effective resistance
r_m = maximum radius of eddy current loop
r_w = radius of wire
V = volume available for eddy current paths

Greek letters

λ = ratio of superconductor volume to winding volume
ρ = resistivity
τ = charge (or discharge) time
ω = angular frequency

REFERENCES

1. W. M. Schwarz, *Intermediate Electromagnetic Theory*, John Wiley and Sons, New York (1964).
2. C. P. Bean, *Phys. Rev. Letters*, **8**:250 (1962).
3. C. P. Bean, "A Research Investigation of the Factors that Affect the Superconducting Properties of Materials," Tech. Rept. No. AFML-TR-65-431 (March 1966).
4. K. P. Jüngst, G. Krafft, and G. Ries, "Measurements on Pulsed Superconducting Magnets," paper presented at Third International Conference on Magnet Technology, May 19–22, 1970, Hamburg, Germany.

APPENDIX B

COMPUTER PROGRAM – L' CALCULATION

```
*A/FRL '/
*WRITE T0T
RETYPE FILE NAME: TPT
DIMENSION T(99),REF(99),R3(99),R4(99),F(99),R31(99),R41(99),TE(99),
      R1ML(99),R1(99),RFTO(99),W(99)
WRITE(1,2)
2 FORMAT(7HBEWARE:,//
      52H        BEFORE PROGRAM IS RUN BE SURE THAT THE VALUES
      20H OF R100TO(LINE 34) ,/
      42HAND RO(LINE 37) ARE CORRECT FOR THIS DATA.)
I=1
R31(M)=0.
WRITE(1,6)
6 FORMAT( 51HREAD IN TIME,R3,R4,AND SENTINEL K.IF K IS NOT ZERO /
      50H1HIS READ LOOP WILL END. ALL VALUES ARE FOR F=100.)
5 READ(0,10)T(I),R3(I),R4(I),K
10 FORMAT(3F8.5,I1)
R2=70.
REF(I)=R2*R3(I)/R4(I)
I=I+1
IF(I-100)11,11,75
11 IF(K)13,5,13
M=0
13 WRITE(1,12)
12 FORMAT(52HREAD IN FREQUENCY,TIME OF MEASUREMENT,CORRESPONDING,/
      52HR3 AND R4,AND L. L MUST BE ZERO OR PROGRAM WILL STOP)
M=M+1
15 READ(0,20)F(M),TE(M),R31(M),R41(M),L
20 FORMAT(F5.1,F5.1,2F8.4,I1)
IF(L)146,25,146
25 IF(TE(M)-T(1))75,30,30
30 J=2
31 IF(TE(M)-T(J))45,40,35
35 J=J+1
IF(J-I)31,75,75
40 REFE=REF(J)
GO TO 50
45 J1=J-1
   REFE=REF(J1)+(REF(J)-REF(J1))/(T(J)-T(J1))*(TE(M)-T(J1))
50 WRITE(1,55)F(M),T(J),REFE
55 FORMAT(2F6.0,F8.5)
REFT(M)=R2*R31(M)/R41(M)
R100TO=5.70777
RFTO(M)=REFT(M)-REFE+R100TO
W(M)=2.*3.14159*F(M)
RO=5.68850
R1MWL=RFTO(M)-RO
R1ML(M)=R1MWL/W(M)
GO TO 13
146 M=1
WRITE(1,155)
155 FORMAT(5H      ,///
      29HRESULTS FOR L' DETERMINATION:,//)
160 WRITE(1,165)
165 FORMAT(48HFREQUENCY   ANG. FREQUENCY       R1ML       RFTO   )
170 WRITE(1,175)F(M),W(M),R1ML(M),RFTO(M)
175 FORMAT(F6.0,6X,F10.0,7X,F9.6,3X,F7.5)
M=M+1
IF(R31(M))170,75,170
75 STOP
1000 END
```

APPENDIX C

COMPUTER PROGRAM – R_0 CALCULATION

```
*WRITE TF1
      DIMENSION T(99),REF(99),R3(99),R4(99),F(99),R31(99),R41(99),TE(99)
      DIMENSION RFTO(100),REFT(100)
      WRITE(1,2)
2     FORMAT(7HBE%ARE:,//
       52H        BEFORE PROGRAM IS RUN BE SURE THAT THE VALUE /
       44H0F R100TO(LINE 35) IS CORRECT FOR THIS DATA.,//)
      R31(M)=0.
      I=1
6     WRITE(1,7)
7     FORMAT( 51HREAD IN TIME,R3,R4,AND SENTINEL K.YF K IS NOT ZERO /
      50HTHIS READ LOOP WILL END. ALL VALUES ARE FOR F=100.)
5     READ(0,10)T(I),R3(I),R4(I),K
10    FORMAT(3F8.5,I1)
      R2=70.
      REF(I)=R2*R3(I)/R4(I)
      I=I+1
      IF(I-100)11,11,75
11    IF(K)13,5,13
      M=0
13    WRITE(1,12)
12    FORMAT(52HREAD IN FREQUENCY,TIME OF MEASUREMENT,CORRESPONDING,/
      52HR3 AND R4,AND L. L MUST BE ZERO OR PROGRAM WILL STOP)
      M=M+1
15    READ(0,20)F(M),TE(M),R31(M),R41(M),L
20    FORMAT(F5.1,F5.1,2F8.4,I1)
      IF(L)70,25,70
25    IF(TE(M)-T(1))75,30,30
30    J=2
31    IF(TE(M)-T(J))44,40,35
35    J=J+1
      IF(J-I)31,75,75
40    REFE=REF(J)
      GO TO 50
44    J1=J-1
45    REFE=REF(J1)+(REF(J)-REF(J1))/(T(J)-T(J1))*(TE(M)-T(J1))
50    WRITE(1,55)F(M),T(J),REFE
55    FORMAT(2F6.0,F8.5)
      REFT(M)=R2*R31(M)/R41(M)
      R100TO=5.64361
      RFTO(M)=REFT(M)-REFE+R100TO
      WRITE(1,60)F(M),RFTO(M)
60    FORMAT(2HF=,F5.1,6X,5HRF10=,F8.5)
      WRITE(1,66)
66    FORMAT(42HREAD IN KRO. IF KRO IS NOT ZERO EXIT LOOP.)
      READ(0,65)KRO
65    FORMAT(I2)
      IF(KRO)70,13,70
70    M=1
      WRITE(1,75)
75    FORMAT(5H      ,///
      29HRESULTS FOR RO DETERMINATION:,//
      37HFREQUENCY     R31        R41         RFTO ,/)
71    WRITE(1,76)F(M),R31(M),R41(M),RFTO(M)
76    FORMAT(F7.0,5X,F5.2,3X,F7.3,3X,F7.5)
      M=M+1
      IF(F(M))71,72,71
72    STOP
      END
```

DISTRIBUTION FOR MERADCOM REPORT 2191

No. Copies	Addressee
	Department of Defense
1	Director, Technical Information Defense Advanced Research Projects Agency 1400 Wilson Blvd Arlington, VA 22209
1	Director Defense Nuclear Agency ATTN: STTL Washington, DC 20305
12	Defense Documentation Center Cameron Station Alexandria, VA 22314
	Department of the Army
6	Commander US Army Materiel Development and Readiness Command ATTN: DRCRD-WB DRCRD-T DRCRD-J DRCRD-O DRCRD-G DRCRD-FP 5001 Eisenhower Ave Alexandria, VA 22333
1	Commander, HQ TRADOC ATTN: ATEN-ME Fort Monroe, VA 23651
1	HQDA (DAMA-AOA-M) Washington, DC 20310
1	HQDA (DALO-TS M-P) Washington, DC 20310
1	HQDA (DAEN-RDL) Washington, DC 20314
1	HQDA (DAEN-MCE-D) Washington, DC 20314
1	Director Army Materials and Mechanics Research Center ATTN: DRXMR-STL Technical Library Watertown, MA 02172

No. Copies	Addressee
1	Director US Army Materiel Systems Analysis Agency ATTN: DRXSY-CM Aberdeen Proving Ground, MD 21005
1	Commander US Army Troop Support & Aviation Materiel Readiness Command ATTN: DRSTS-KTE 4300 Goodfellow Blvd St Louis, MO 63120
1	Commander US Army Electronics Research and Development Command ATTN: DRSEL-GG-TD Fort Monmouth, NJ 07703
2	Engineer Representative US Army Standardization Group, UK Box 65, FPO New York 09510
1	Learning Resources Center US Army Engineer School Bldg 270 Fort Belvoir, VA 22060
1	Commandant US Army Command and General Staff College ATTN: ATSW-RI-L Fort Leavenworth, KS 66027
1	Commander and Director USAFESA ATTN: FESA-RTD Fort Belvoir, VA 22060
	MERADCOM
1	Commander Technical Director Assoc Tech Dir/R&D Assoc Tech Dir/Engrg & Acq Assoc Tech Dir/Matl Asmt Assoc Tech Dir/Tech Asmt CIRCULATE

No. Copies	Addressee
1	Chief, Countermine Lab Chief, Energy & Water Res Lab Chief, Electrical Power Lab Chief, Camouflage & Topo Lab Chief, Marine & Bridge Lab Chief, Mech & Const Eqpt Lab Chief, Counter Intrusion Lab Chief, Product Assur & Testing Lab Chief, Material Technology Lab Chief, TARSO CIRCULATE
12	Elect Equipment Div, Elect Power Lab
3	Tech Reports Ofc
3	Security Ofc
2	Tech Library
1	Requirements & Programs Ofc
1	Public Affairs Ofc
1	Legal Ofc
	Department of the Navy
1	Director, Physics Program (421) *Office of Naval Research* Arlington, VA 22217
1	Director Naval Research Laboratory ATTN: Code 2627 Washington, DC 20375
	Department of the Air Force
1	HQ USAF/RDPS (Mr. Allan Eaffy) Washington, DC 20330

DEPARTMENT OF THE ARMY
U. S. ARMY MOBILITY EQUIPMENT
RESEARCH AND DEVELOPMENT COMMAND
FORT BELVOIR, VIRGINIA 22060

OFFICIAL BUSINESS

PENALTY FOR PRIVATE USE, $300

POSTAGE AND FEES PAID
U. S. DEPARTMENT OF THE ARMY
DOD-314

THIRD CLASS MAIL